A Unified Scheme to Solving Complex-valued Ratio Distribution with Application to Statistical Inference for Frequency Response Functions and Transmissibility Functions

Wang-Ji Yan[1], Meng-Yun Zhao[2], Wei-Xin Ren[2], Micheal Beer[3], Dimitrios Chronopoulos[4]

[1]*State Key Laboratory of Internet of Things for Smart City and Department of Civil and Environmental Engineering, University of Macau, China*

[2]*Department of Civil Engineering, Hefei University of Technology, Anhui, China*

[3]*Institute for Risk and Reliability, Leibniz Universität Hannover, Germany*

[4]*Institute for Aerospace Technology & The Composites Group, The University of Nottingham, United Kingdom*

Abstract: Complex-valued ratio distributions arise in many scientific and engineering domains such as statistical inference for frequency response functions (FRFs) and transmissibility functions (TFs) in structural health monitoring. When solving the distribution properties for complex ratio random variables through the definition of probability density function (PDF), the problem is usually accompanied by complicated derivatives. In this study, a unified scheme to solve complex ratio random variables is proposed for the case when it is highly non-trivial or impossible to discover a closed-form solution, such as for complex-valued t ratio distributions. Based on the probability transformation principle in the complex domain, a unified formula is derived by reducing the concerned problem into multidimensional integrals, which can be solved by advanced numerical techniques. A fast Sparse-Grid Quadrature (SGQ) rule by constructing multivariate quadrature formulas using the combinations of tensor products of suitable one-dimensional formulas is utilized to improve the computational efficiency by avoiding the curse of integral dimensionality. The unified methodology can efficiently calculate the PDF of a ratio random variable with its denominator and nominator specified by arbitrary probability distributions including Gaussian or non-Gaussian ones, correlated or independent random variables, as well as bounded or unbounded ratio random variables. The unified scheme

is applied to uncertainty quantification for FRFs and TFs, and the efficiency of the proposed scheme is verified by using the vibration testing field data conducted on a simply-supported beam, as well as onAlamosa Canyon Bridge.

Keywords: Probability density function; Frequency response function; Transmissibility function; Complex ratio distribution; Sparse-Grid Quadrature rule

1 Introduction

In engineering science, the ratio function defined as the quotients of two variables plays an important role in various fields. Uncertainty quantification for ratio random variables arises in many applied problems such as eigenvalue ratio distribution for cooperative spectrum sensing in cognitive radio [1], mass to energy ratios in nuclear physics, Mendelian inheritance ratios in genetics, and inventory ratios in economics, etc. [2]. Probability density function (PDF) is usually regarded as one of the most valued ways to quantify the uncertainty comprehensively [3-5]. As popular statistical models, the Cauchy distribution, t-distribution and F-distribution are commonly-taught ratio distribution in statistical textbooks. Over the past few decades, the PDF of ratio random variables including the Gaussian distribution family [6-8], t-distribution family [9,10], Weibull family [11], chi-square family [12], gamma family [13], beta family [14] and Bessel family [15], etc. have been studied extensively by a number of researchers.

It is worth noting that most of the efforts mentioned in the above are devoted to real-valued cases, while the distribution properties of ratios of complex random variables are not well developed. In [16], the authors showed that the symbol error rate (SER) of a flat fading communications system can be expressed in closed form by expressing the demodulator outputs as random variable that have a complex ratio distribution. In the field of dynamics, the characterization functions including frequency response function (FRF) [17-20] and transmissibility function (TF) [21-25] defined as the ratios of two frequency-domain responses also fall into the category of complex ratio random variables. As the most prevalent frequency domain tools, FRF represents the input-output relationships, while TF is a mathematical representation of the output-to-output relationship. Due to their clear physical interpretations, FRFs and TFs are of fundamental importance in damage detection [26-31], modal analysis [32-35], model updating [36, 37], operational path analysis [38],vibration isolation [39], etc.

It is worth mentioning here that both FRF and TF are estimated based on FFT coefficients which inevitably involve different sources of uncertainties due to the inherent randomness of excitation, the variability of environmental conditions, as well as the numerical errors caused by discrete signals [40]. Therefore, the results of complex ratio functions obtained via deterministic analysis methods without considering randomness related to FFT coefficients involved in engineering can deviate the actual values significantly. As a result, quantifying the uncertainty for FRF and TF has been a fundamental way of improving the robustness of real applications.

Different approaches have been proposed to investigate the uncertainty of FRFs and TFs. Mao and Todd [20, 21] presented an analytical probabilistic model to quantify the uncertainty of FRFs and TFs using a Gaussian bivariate statistical model. However, the models are still restricted to real-valued domain. Over the past few years, new theorems on circularly-symmetric complex Gaussian ratio distribution [22] as well as generalized complex Gaussian ratio distribution [19] have been proven mathematically to quantify the statistical distribution of FRF and TF. Unfortunately, these probabilistic models can only be utilized to characterize the uncertainty of FRFs and TFs when FFT coefficients follow complex Gaussian distribution. Recent research has revealed that the FFT coefficients may deviate from Gaussian distribution [41] and the complex Gaussian ratio distribution may cause unexpected errors in uncertainty quantification. Therefore, there is a need to propose a more versatile way to compute the ratio distribution with its numerator and denominator following arbitrary complex-valued probability distributions.

In this study, a unified scheme is presented to efficiently calculate the PDF of a ratio random variable with its denominator and numerator specified by arbitrary distributions. Making use of the probability density transformation principle in the complex domain, a unified formula is derived for complex ratio distribution by reducing the concerned problem into

multidimensional integrals. When it is difficult or impossible to discover a closed-form solution, one ought to resort to numerical algorithms. For the Gaussian quadrature rule, the number of points to be calculated increases exponentially with the dimension of integrals, leading to excessive computational burden. In this study, a novel SGQ formula based on the Smolyak rule [42] will be employed to address the curse of dimensionality. The sparse-grid method utilizes a linear combination of lower-level tensor products of univariate quadrature rules to approximate multivariate integrals [43,44]. Then the univariate quadrature point sets are extended to form a multi-dimensional grid using the sparse-grid theory [45-47]. The locations and weights of the univariate quadrature points corresponding to a range of accuracy levels can be determined by asymptotic approximations. Unlike the Gaussian quadrature formula, the accuracy of the SGQ rule can be flexibly controlled. The method proposed in this paper can tackle various cases including the ratio of Gaussian and non-Gaussian random variables, correlated and independent random variables as well as infinite and finite interval random variables.

The organization of this paper is as follows. Section 2 presents the theoretical background and the unified formula for complex ratio distribution expressed in terms of multidimensional integrals based on the principle of probability transformation in the complex domain. The SGQ formula based on the Smolyak rule is introduced in Section 3 to address the computational burden of multidimensional integrals involved in the unified formula of complex ratio distribution. The theoretical findings proposed in Section 2 and Section 3 are then utilized to infer the statistics of FRFs and TFs in Section 4. Two case studies are conducted in Section 5 to verify the unified formula of complex ratio distribution solved using SGQ strategy.

2 A Unified Scheme to Solving Complex Ratio Distribution

2.1 Some basic definitions

This study concerns the distribution of $\mathrm{Z} \in \mathbb{C}$ formulated as the ratio of two complex-valued random variables:

$$\mathrm{Z} = \frac{U}{V} = \frac{U^{\Re} + \mathbf{i}U^{\Im}}{V^{\Re} + iV^{\Im}} \tag{1}$$

where $\mathbf{i} = \sqrt{-1}$; $U^{\Re}$ and $U^{\Im}$ denote the real and imaginary parts of U, while $V^{\Re}$ and $V^{\Im}$ denote the real and imaginary parts of V.

In the available references, the most common way of computing the distribution of ratio random variables is based on the definition of PDF by taking the derivative of the Cumulative Distribution Function (CDF) [16]. The complex-valued random variable Z is defined as $\mathrm{Z} = \mathrm{Z}^{\Re} + \mathbf{i}\mathrm{Z}^{\Im}$, where $\mathrm{Z}^{\Re}$ and $\mathrm{Z}^{\Im}$ are a pair of real-valued random variables. Z is identified with the joint-distribution of its real and imaginary parts $\left[\mathrm{Z}^{\Re}, \mathrm{Z}^{\Im}\right]$ being expressed as [48]:

$$\mathrm{F}_{\mathrm{Z}}\left(z\right) = \mathrm{F}_{\mathrm{Z}^{\Re},\mathrm{Z}^{\Im}}\left(z^{\Re}, z^{\Im}\right) = p\left(\mathrm{Z}^{\Re} \le z^{\Re}, \mathrm{Z}^{\Im} \le z^{\Im}\right) \tag{2}$$

where $\mathrm{F}_{\mathrm{Z}}(z)$ and $\mathrm{F}_{\mathrm{Z}^{\Re},\mathrm{Z}^{\Im}}\left(z^{\Re}, z^{\Im}\right)$ are the CDF of complex random variable Z and joint-distribution function of bivariate random vector $\left[\mathrm{Z}^{\Re}, \mathrm{Z}^{\Im}\right]$, respectively. If $\mathrm{F}_{\mathrm{Z}^{\Re},\mathrm{Z}^{\Im}}\left(z^{\Re}, z^{\Im}\right)$ is differentiable in $z^{\Re}$ and $z^{\Im}$, the following function is defined as PDF of the random variable z [16]:

$$p_{\mathrm{Z}}(z) = p_{\mathrm{Z}^{\Re},\mathrm{Z}^{\Im}}\left(z^{\Re}, z^{\Im}\right) = \frac{\partial^2}{\partial z^{\Re} \partial z^{\Im}} \mathrm{F}_{\mathrm{Z}^{\Re},\mathrm{Z}^{\Im}}(z^{\Re}, z^{\Im}) \tag{3}$$

From the above formulas, one can find that the solution involves complicated formulas of CDF and partial derivatives. To avoid the difficulty of computing the CDFs and its partial derivatives, the principle of probabilistic transformation of random variables in the complex domain will be used in this study. As a result, complex ratio random variable following arbitrary distribution can reduce to a unified formula involving multidimensional integrals.

2.2 Linear probabilistic transformation in the complex domain

In the real-valued domain, if an n_o-variate random vector $\mathbf{X}=\left(X_1,X_2,\cdots,X_{n_o}\right)^T$ has a joint PDF $p_{\mathbf{X}}\left(\mathbf{x}\right)$ with the value $\mathbf{x}=\left(x_1,x_2,\cdots,x_{n_o}\right)^T$, while a one-to-one and onto function is denoted by $\mathbf{s}=\mathrm{G}\left(\mathbf{x}\right)=\left(\mathrm{G}_1\left(\mathbf{x}\right),\mathrm{G}_2\left(\mathbf{x}\right),\cdots,\mathrm{G}_{n_o}\left(\mathbf{x}\right)\right)^T$; the inverse function of $\mathbf{s}=\mathrm{G}\left(\mathbf{x}\right)$ is denoted by $\mathbf{x}=\mathrm{Q}\left(\mathbf{s}\right)=\mathrm{G}^{-1}\left(\mathbf{s}\right)$. The principle of probabilistic transformation of random vectors states that the PDF of a transformed random vector $\mathbf{s}=\mathrm{G}\left(\mathbf{x}\right)$ is given by [49]:

$$p_{\mathbf{S}}\left(\mathbf{s}\right)=\left|\mathrm{J}_{\mathrm{G}}\left(\mathrm{Q}\left(\mathbf{s}\right)\right)\right|^{-1}p_{\mathbf{X}}\left(\mathrm{Q}\left(\mathbf{s}\right)\right) \tag{4}$$

where $\mathrm{J}_{\mathrm{G}}\left(\mathrm{Q}\left(\mathbf{s}\right)\right)$ denotes the Jacobian matrix given by:

$$\mathrm{J}_{\mathrm{G}}\left(\mathrm{Q}\left(\mathbf{s}\right)\right)=\partial\left(\mathrm{G}_1,\mathrm{G}_2,\cdots,\mathrm{G}_{n_o}\right)\Big/\partial\left(x_1,x_2,\cdots,x_{n_o}\right) \tag{5}$$

Assume that two complex-valued random vectors $\mathbf{R}$ relates to $\boldsymbol{\Theta}$ through a linear transformation:

$$\mathbf{R}=\mathbf{W}\boldsymbol{\Theta} \tag{6}$$

Where $\mathbf{R}=\mathbf{R}^{\Re}+\mathbf{i}\mathbf{R}^{\Im}$, $\mathbf{W}=\mathbf{W}^{\Re}+\mathbf{i}\mathbf{W}^{\Im}$ and $\boldsymbol{\Theta}=\boldsymbol{\Theta}^{\Re}+\mathbf{i}\boldsymbol{\Theta}^{\Im}$. The above equation can be rearranged as:

$$\begin{Bmatrix}\mathbf{R}^{\Re}\\ \mathbf{R}^{\Im}\end{Bmatrix}=\begin{bmatrix}\mathbf{W}^{\Re} & -\mathbf{W}^{\Im}\\ \mathbf{W}^{\Im} & \mathbf{W}^{\Re}\end{bmatrix}\begin{Bmatrix}\Theta^{\Re}\\ \Theta^{\Im}\end{Bmatrix} \tag{7}$$

A complex random vector is specified by the joint-distribution of its real and imaginary parts, i.e. $p_{\mathbf{R}}\left(\mathbf{r}\right)=p_{\mathbf{R}^{\Re},\mathbf{R}^{\Im}}\left(\mathbf{r}^{\Re},\mathbf{r}^{\Im}\right)$ and $p_{\Theta}\left(\theta\right)=p_{\Theta^{\Re},\Theta^{\Im}}\left(\theta^{\Re},\theta^{\Im}\right)$. According to the principle of probabilistic transformation of real random vectors, the joint PDF of $\left(\mathbf{R}^{\Re},\mathbf{R}^{\Im}\right)$ is equal to [23]:

$$p_{\mathbf{R}}\left(\mathbf{r}\right)=p_{\mathbf{R}^{\Re},\mathbf{R}^{\Im}}\left(\mathbf{r}^{\Re},\mathbf{r}^{\Im}\right)=\left|\mathrm{J}_{\mathrm{W}}\right|^{-1}p_{\Theta}\left(\theta\right) \tag{8}$$

where $\mathrm{J}_{\mathrm{W}}=\begin{bmatrix}\mathbf{W}^{\Re} & -\mathbf{W}^{\Im}\\ \mathbf{W}^{\Im} & \mathbf{W}^{\Re}\end{bmatrix}$, and correspondingly, the determinant $\left|\mathrm{J}_{\mathrm{W}}\right|$ is given by:

$$\left|\mathrm{J}_{\mathrm{W}}\right|=\begin{vmatrix}\mathbf{W}^{\Re} & -\mathbf{W}^{\Im}\\ \mathbf{W}^{\Im} & \mathbf{W}^{\Re}\end{vmatrix}=\left|\mathbf{w}\mathbf{w}^{*}\right|=\left|\mathbf{w}\right|^{2} \tag{9}$$

Substituting Eq.(9) into Eq. (8) leads to the PDF of $\mathbf{R}$:

$$p_{\mathbf{R}}\left(\mathbf{r}\right)=\left|\mathbf{w}\right|^{-2}p_{\Theta}\left(\theta\right) \tag{10}$$

2.3 The unified formula of complex ratio distribution

Since the complex ratio random variable $\mathrm{Z}=\frac{U}{V}$ is evolved from complex random variables $\{V,U\}^{T}\in\mathbb{C}^{2}$, it is intuitive to conceive the idea of deriving the PDF of Z using the principle of probabilistic transformation of a random vector in the complex domain introduced in the last section. However, the application of the principle of probabilistic transformation of random vectors should formulate a functional relationship between Z and $\{V,U\}^{T}$. To realize such a transformation, an auxiliary variable V is herein introduced to ensure that Z and $\{V,U\}^{T}$ have the same order:

$$\begin{Bmatrix}V\\ \mathrm{Z}\end{Bmatrix}=\begin{bmatrix}1 & 0\\ 0 & V^{-1}\end{bmatrix}\begin{Bmatrix}V\\ U\end{Bmatrix} \tag{11}$$

Using Eq.(6) with $\mathbf{R}=\begin{Bmatrix}V & \mathrm{Z}\end{Bmatrix}^{T}$, $\mathbf{W}=\begin{bmatrix}1 & 0\\ 0 & V^{-1}\end{bmatrix}$, and $\Theta=\begin{Bmatrix}V & U\end{Bmatrix}^{T}$, a linear transformation between Z and $\Theta=\begin{Bmatrix}V & U\end{Bmatrix}^{T}$ is realized. According to Eq.(11), one has $\left|\mathbf{w}\right|=\left|v\right|^{-2}$. Therefore, the PDF of $\mathbf{R}=\begin{Bmatrix}V & \mathrm{Z}\end{Bmatrix}^{T}$ can be derived based on Eq.(10):

$$p_{\mathbf{R}}\left(\mathbf{r}\right)=\left|v\right|^{-2}p_{\Theta}\left(\theta\right) \tag{12}$$

It is noted that the random vector $\Theta=\left\{V \quad U\right\}^T$ can be expressed as a function in terms of V and $\tilde{Z}=\left\{1 \quad Z\right\}^T$, i.e.:

$$\boldsymbol{\Theta}=V\left\{1 \quad \frac{U}{V}\right\}^T=V\tilde{Z} \tag{13}$$

By substituting Eq. (13) into (12) leads to the joint PDF of V and Z, i.e., $p_{\mathbf{R}}\left(\mathbf{r}\right)=\left|v\right|^{-2}p_{\Theta}\left(v\tilde{z}\right)$. As a result, the PDF of Z can be easily obtained by marginalizing out the variable V as:

$$p_{Z}\left(z\right)=\int_{\Omega^{v}}p_{\mathbf{R}}\left(\mathbf{r}\right)dv=\int_{\Omega^{v}}\left|v\right|^{-2}p_{\Theta}\left(v\tilde{z}\right)dv=\int_{\Omega^{v^{\Re}}}\int_{\Omega^{v^{\Im}}}\left|v\right|^{2}p_{\Theta}\left(v\tilde{z}\right)dv^{\Re}dv^{\Im} \tag{14}$$

where $\tilde{\mathbf{z}}=\left\{1 \quad \mathbf{z}\right\}^T$ and $\Omega^{(\bullet)}$ denotes the integration interval of the variable $\left(\bullet\right)$.

Based on the formula of Z, one can further calculate the marginal PDFs of the real and imaginary part of Z by marginalizing out $Z^{\Im}$ and $Z^{\Re}$, respectively:

$$p_{Z^{\Re}}\left(z^{\Re}\right)=\int_{\Omega^{v^{\Re}}}\int_{\Omega^{v^{\Re}}}\int_{\Omega^{z^{\Im}}}\left|v\right|^{2}p_{\Theta}\left(v\tilde{z}\right)dv^{\Re}dv^{\Im}dz^{\Im} \tag{15a}$$

$$p_{Z^{\Im}}\left(z^{\Im}\right)=\int_{\Omega^{v^{\Re}}}\int_{\Omega^{v^{\Re}}}\int_{\Omega^{z^{\Re}}}\left|v\right|^{2}p_{\Theta}\left(v\tilde{z}\right)dv^{\Re}dv^{\Im}dz^{\Re} \tag{15b}$$

According to the definition of expectation, the statistical moments of $Z^{\Re}$ and $Z^{\Im}$, such as mean can be obtained by integrating $p_{Z^{\Re}}\left(z^{\Re}\right)$ and $p_{Z^{\Im}}\left(z^{\Im}\right)$ over the domain of $Z^{\Re}$ and $Z^{\Im}$:

$$E\left(z^{\Re}\right)=\int_{\Omega^{v^{\Re}}}\int_{\Omega^{v^{\Re}}}\int_{\Omega^{z^{\Im}}}\int_{\Omega^{z^{\Re}}}\left|v\right|^{2}p_{\Theta}\left(v\tilde{z}\right)dv^{\Re}dv^{\Im}dz^{\Im}dz^{\Re} \tag{16a}$$

$$E\left(z^{\Im}\right)=\int_{\Omega^{v^{\Re}}}\int_{\Omega^{v^{\Re}}}\int_{\Omega^{z^{\Re}}}\int_{\Omega^{z^{\Im}}}\left|v\right|^{2}p_{\Theta}\left(v\tilde{z}\right)dv^{\Re}dv^{\Im}dz^{\Re}dz^{\Im} \tag{16b}$$

Therefore, the unified formula of the PDF of Z, the marginal PDFs of $Z^{\Re}$ and $Z^{\Im}$ as well as the statistical moments of $Z^{\Re}$ and $Z^{\Im}$ such as the mean can be simply determined by

substituting the joint PDF of $\Theta=\left\{V \quad U\right\}^{T}$ into (14)-(16) and replacing the random vector $\boldsymbol{\Theta}$ by its equivalence $V\tilde{Z}$.

3 Fast Numerical Soltuion incorporating SGQ Rule

Whether the closed-form solutions of Eq.(14)-(16) is available or not highly depend on the formula $p_{\Theta}\left(v\tilde{z}\right)$. Obviously, it is non-trivial or impossible to derive the closed-form solutions of $p_{Z}\left(z\right)$ for arbitrary ratio $p_{\Theta}\left(v\tilde{z}\right)$ without following Gaussian distribution , and one should resort to numerical algorithms.

3.1 Gauss quadrature rule

In cases where the integral is univariate, Gaussian quadrature and related approaches are potentially powerful, which is approximated by summing up some items of weighted integrand evaluated at the Gauss points (abscissas) [50,51]:

$$I_{1}=\int_{\Omega^{x}} g\left(x\right)dx \approx \sum_{i=1}^{n_{r}} w_{i} g\left(\tilde{x}_{i}\right) \tag{17}$$

where n_{r} is the quadrature order (equal to the number of abscissas), $\tilde{x}_{i}$ are abscissas (Gauss points), and w_{i} are weights (Gauss weights); Ω^{x} denotes the integral region.

The univariate quadrature rule can be extended to multidimensional domain by using the product rule, which in turn results in an exponential rise in multivariate quadrature points. The Gauss quadrature formula for a D-dimensional integral is given by [50,51]:

$$I_{D}=\int_{\Omega^{x_{D}}}\cdots\int_{\Omega^{x_{1}}} g\left(x_{1},x_{2},\cdots,x_{D}\right)dx_{1}\cdots dx_{D} \approx \sum_{i_{D}}^{n_{i_{D}}}\cdots\sum_{i_{1}=1}^{n_{i_{1}}} w_{i_{1}}\cdots w_{i_{D}} g\left(\tilde{x}_{i_{1}},\tilde{x}_{i_{2}},\cdots,\tilde{x}_{i_{D}}\right) \tag{18}$$

where $\left(n_{i_{1}}\cdots n_{i_{D}}\right)$ denote the quadrature order (the number of abscissas) used in $\left(\tilde{x}_{1},\tilde{x}_{2},\cdots,\tilde{x}_{n_{d}}\right)$ directions; $\left(\tilde{x}_{i_{1}},\tilde{x}_{i_{2}},\cdots,\tilde{x}_{i_{D}}\right)$ are Gauss points; $\left(w_{i_{1}}\cdots w_{i_{n_{d}}}\right)$ are the corresponding weights and

Ω^{x_i} denotes the integral region of the i-th parameter x_i. It is worth mentioning here that the subscripts involved in 'I' denote the integral dimension.

3.2 SGQ rule

As is seen from Eq. (18), the total number of points in the Gauss quadrature rule to be calculated increases exponentially with the integral dimension. The curse of dimensionality can hinder the applicability. To address the critical issue, Smolyak-type quadrature formula which is more computationally efficient than the usual multidimensional Gauss quadrature rule will be utilized in this study. The Smolyak quadrature formula uses Gauss quadrature rule for generating univariate quadrature points and its multidimensional extension is obtained using the Smolyak rule [42] utilizing a linear combination of lower-level tensor products of univariate quadrature rules to approximate multivariate integrals. Like the product rule, it combines univariate quadrature rules, so it is very general and straightforward to-implement. Unlike the product rule, its computational cost does not rise exponentially with the number of considered variables. This gives an additional advantage to the SGQ method, i.e. that the accuracy of its estimation can be defined separately.

Definition of quadrature approximation: As indicated in Eq.(17), the one-dimensional quadrature rule delivers the exact value of the integral I_1 if $g(x)$ is a polynomial of a given order. Here we can define a sequence of single-dimension quadrature rules $\Lambda=\{\Lambda_l, l\in\square\}$ so that the order of polynomial increases with the accuracy level l. The quadrature approximation Λ_l is given by [44]:

$$\Lambda_l = \sum_{\tilde{x}\in X_l} g(\tilde{x}) w_l(\tilde{x}) \tag{19}$$

Each rule Λ_l specifies n_l nodes $\mathrm{X}_l = \left[\tilde{x}_1, \tilde{x}_2, \cdots, \tilde{x}_{n_l}\right]$ and a corresponding weight function $w_l\left(\tilde{x}\right)$.

Definition of difference of the quadrature approximation: When increasing the level of accuracy from l-1 to l, the difference of the quadrature approximation is defined as [44]:

$$\Delta_l = \Lambda_l - \Lambda_{l-1} \tag{20}$$

Definition of accuracy level sequences: For the convenience of derivation, a new vector $\boldsymbol{\Xi} \triangleq \left\{l_1, l_2, \ldots, l_D\right\}$ is formulated with each of its entries l_i denoting the accuracy level of the univariate-dimensional quadrature rule for the i-th variable. For any nonnegative integer q, the set of accuracy level sequences $\mathbb{N}_q^D$ is defined as [44]:

$$\begin{cases} \mathbb{N}_q^D = \left\{\Xi : \sum_{i=1}^{D} l_i = D + q\right\}, \text{for } q \geq 0 \\ \mathbb{N}_q^D = \varnothing \qquad\qquad\qquad\quad , \text{ for } q < 0 \end{cases} \tag{21}$$

where $\varnothing$ is the empty set; q has the range of $L - D \leq q \leq L - 1$. For $\mathbb{N}_2^3$, $\mathbb{N}_2^2 = \left\{\left[1,3\right], \left[2,2\right], \left[3,1\right]\right\}$.

The Smolyak rule: Making full use of the definitions indicated in Eq. (19)-(21), the Smolyak rule states that a numerical approximation with accuracy level $L \in \mathbb{N}$ for D-dimensional integrals denoted by I_D^L can be expressed as [43-46]:

$$I_D^L\left(g\right) = \sum_{q=0}^{L-1} \sum_{\Xi \in \mathbb{N}_q^D} \left(\Delta_{l_1} \otimes \Delta_{l_2} \otimes \cdots \otimes \Delta_{l_D}\right)\left(g\right) \tag{22}$$

where $\otimes$ stands for the tensor product; the auxiliary parameter q and $\mathbb{N}_q^D$ are defined in Eq.(21).

Wasilkowski et al. [43] proved that Eq. (22) can be explicitly written as

$$I_D^L\left(g\right) = \sum_{q=L-D}^{L-1} \left(-1\right)^{L-1-q} C_{D-1}^{L-1-q} \sum_{\Xi \in \mathbf{N}_q^D} \left(\Lambda_{l_1} \otimes \Lambda_{l_2} \otimes \cdots \otimes \Lambda_{l_D}\right)\left(g\right) \tag{23}$$

where C_{D-1}^{L-1-q} denotes the binomial coefficient with $C_{D-1}^{L-1-q} = \begin{pmatrix} D-1 \\ L-1-q \end{pmatrix}$. By substituting Eq. (18) into Eq.(23) leads to [43-46]:

$$I_D^L(g) = \sum_{q=L-D}^{L-1} \sum_{\Xi \in \square_q^D} \sum_{\tilde{x}_1 \in X_{l_1}} \cdots \sum_{\tilde{x}_D \in X_{l_D}} (-1)^{L-1-q} C_{D-1}^{L-1-q} \times g(\tilde{x}_1, \cdots, \tilde{x}_D) \prod_{i=1}^{D} w_{l_i}(\tilde{x}_i) \tag{24}$$

where X_{l_i} is the set of quadrature points for single dimension quadrature rule Λ_{l_i}; $[\tilde{x}_1, \cdots, \tilde{x}_D]^T$ is a D-dimensional vector of SGQ points where $\tilde{x}_j \in X_{l_j}$; $w_{l_i}(\tilde{x}_i)$ are the weightings in Λ_{l_i} associated with $\tilde{x}_j \in X_{l_j}$. Eq. (24) boils down to a weighted sum of function evaluations $f(\mathbf{x})$.

The sets of nodes $[\tilde{x}_1, \cdots, \tilde{x}_D]^T$ are determined by the relevant combinations of nodes of univariate quadrature rules Λ_{l_i}, where the levels of accuracy in each dimension are determined by $\Xi \in \square_q^D$ and $L-D \le q \le L-1$. The corresponding weights are $(-1)^{L-1-q} C_{D-1}^{L-1-q} \prod_{i=1}^{D} w_{l_i}(\tilde{x}_i)$. The final set of the SGQ points are given as:

$$X_D^L = \bigcup_{q=L-D}^{L-1} \bigcup_{\Xi \in \square_q^D} (X_{l_1} \otimes X_{l_2}, \cdots \otimes X_{l_D}) \tag{25}$$

where $\bigcup(\square)$ represents union of the individual SGQ points. The procedures of generating points and weights from the univariate quadrature point sets using the Smolyak rule are shown in Table 1. The MATLAB implementation of the SGQ algorithm is referred to the Appendix of [52]. The quadrature points required to be generated for conventional Gaussian quadrate rule and SGQ rule are compared in Table 2, which clearly shows that the SGQ rule can reduce the quadrature points, thus improving the computation efficiency significantly.

1

Table 1: The procedures of generating SGQ points and weights [42]

Input: dimension D, accuracy level L

Output: matrix χ containing the SGQ nodes with the element of χ_i,
vector W containing the respective weights with the element of W_i;

Step 1

FOR $l = 1:L$

- Select the quadrature point set of the univariate Gaussian quadrature rule Λ_{l_i} and the corresponding weight w_{l_i};
- Determine $\mathrm{X}_{l_1}, \mathrm{X}_{l_2}, \cdots, \mathrm{X}_{l_D}$ and the corresponding weights of the points;

END

Step 2

FOR $q = L - D : L - 1$

- Determine $\square_q^n$ following the equation: $\sum_{i=1}^{D} l_i = D + q$ with $1 \le l_i < n + q$

FOR each element of $\Xi \square \{l_1, l_2, \ldots, l_D\}$ in $\square_q^n$

- Form $\left(\mathrm{X}_{l_1} \otimes \mathrm{X}_{l_2}, \cdots \otimes \mathrm{X}_{l_D}\right)$;

FOR each point $\left[x_1, \cdots, x_D\right]^T \left(x_i \in \mathrm{X}_{l_i}\right)$ in $\left(\mathrm{X}_{l_1} \otimes \mathrm{X}_{l_2} \cdots \otimes \mathrm{X}_{l_D}\right)$

IF the point is new

- Add the point to χ;
- Assign a new index i to this point;
- Set the weights of χ_i as $W_i = (-1)^{L-1-q} C_{n-1}^{L-1-q} \prod_{j=1}^{n} \hat{w}_{s_j} \left(\hat{w}_{s_j} \in \hat{w}\right)$;

ELSE (the points already exists)

- Update the weight by $W_i = W_i + (-1)^{L-1-q} C_{n-1}^{L-1-q} \prod_{j=1}^{n} \hat{w}_{s_j} \left(\hat{w}_{s_j} \in \hat{w}\right)$;

END IF

END FOR

END FOR

END FOR

Table 2: The number of quadrature points required by two quadrature rules under consideration

Integral dimension n	Accuracy level L	Number of quadrature points	
		Gaussian quadrature	SGQ
2	3	49	17
	4	169	45
	5	441	97
3	3	343	35
	4	2197	105
	5	9261	297
	3	2401	55

4	4	28561	207
	5	194481	681

3.3 Summurry of procedures

The main procedures for calculating the PDF of arbitrary complex-valued ratio distributions using the unified scheme are summarized in Table 3.

Table 3: The procedures of calculating the PDF of complex-valued ratio distribution with the unified scheme

Step	Procedures
1	Formulate $p_{\Theta}\left(v\tilde{z}\right)$ through replacing Θ by $V\tilde{Z}$
2	Formulate the unified formula by substituting $p_{\Theta}\left(v\tilde{z}\right)$ into (14)-(16)
3	Generate SGQ points and weights following Table 1
4	Calculate the multidimensional integral involved in (14)-(16) by using Eq.(24) based on the SGQ points and weights.

4 Applications to Statistical Inference for FRF and TF

4.1 Definition of FRF and TF

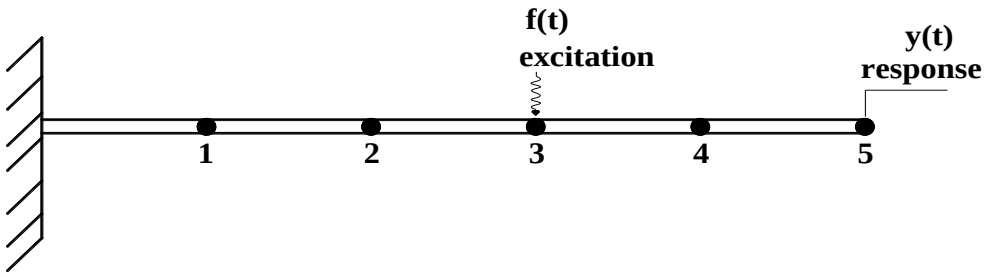

Fig. 1: Typical diagram of an dynamic system subject to a single input

Of interest now are problems involving a single-input dynamical system shown in Fig.1. For a multi-degree-of-freedom (MDOF) linear system, it is assumed that a single input is applied on the i-th DOF, and the response measurements are available for n_o measured

DOFs. The time history can be modeled as a realization of stochastic vector process, which is denoted by $f_i(t)$ and $\mathbf{y}(t)=\left\{y_0(t),y_1(t),\cdots,y_{n_o}(t)\right\}^T$ for the input and output, respectively. The corresponding discrete-time stochastic vector processes of $f_i(t)$ and $y_j(t)$ are denoted by $f_i(n)=\left\{f_i(0),f_i(\Delta t),\cdots,f_i((N-1)\Delta t)\right\}^T$ and $y_j(n)=\left\{y_j(0),y_j(\Delta t),\cdots,y_j((N-1)\Delta t)\right\}^T$, which correspond to the sampled data in real applications. At frequency ω_k, the discrete Fourier transforms of the input and output measures are defined as:

$$\begin{cases} F_i^{(\omega_k)}=F_i^{\Re}(\omega_k)+\mathbf{i}F_i^{\Im}(\omega_k)=\sqrt{\Delta t/2\pi N}\sum_{n'=0}^{N-1}f_i(n)e^{(-\mathrm{i}\omega_k n\Delta t)} \\ Y_j^{(\omega_k)}=Y_j^{\Re}(\omega_k)+\mathrm{i}Y_j^{\Im}(\omega_k)=\sqrt{\Delta t/2\pi N}\sum_{n'=0}^{N-1}y_j(n)e^{(-\mathrm{i}\omega_k n\Delta t)} \end{cases} \tag{26}$$

where $\mathrm{i}^2=-1$, $\omega_k=2\pi f_k$, $k=1,2,\cdots,Int(N/2)$, and $\Delta\omega=2\pi/(N\Delta t)$. In this work, '$\omega_k$' shown in a bracket or superscript denotes the frequency point.

As a result, the FRF $H_{ij}^{(\omega_k)}$ reflecting the input-out relationship between $f_i(t)$ and $y_j(t)$, as well as TF $T_{ij}^{(\omega_k)}$ reflecting the output-output relationship between an arbitrary response $Y_j^{(\omega_k)}$ and a reference response $Y_i^{(\omega_k)}$ are defined as:

$$H_{ij}^{(\omega_k)}=Y_j^{(\omega_k)}\Big/F_i^{(\omega_k)} \tag{27a}$$

$$T_{ij}(\omega_k)=Y_j^{(\omega_k)}\Big/Y_i^{(\omega_k)} \tag{27b}$$

As seen from Eq.(27a) and (27b), both FRF and TF are complex-valued ratio random variables composed of both real and imaginary parts which are correlated with each other. As emphasized frequently, one of the core issues in developing probabilistic models for raw FRFs and TFs is to investigate the statistics of the frequency-domain stochastic vector of the input and output, i.e., $\Psi_k=\left[F_i^{(\omega_k)},Y_j^{(\omega_k)}\right]$ or $\Psi_k=\left[Y_i^{(\omega_k)},Y_j^{(\omega_k)}\right]$.

4.2 Probabilistic models of FFT coefficients in the complex domain

The statistics of the FFT coefficients have been studied extensively over the past few decades. One can propose different probabilistic models to quantify the uncertainty of FFT coefficients, and the performance of different probabilistic models may be dependent on the nature of excitation, the length of time history, etc. Here, two probabilistic models including the complex Gaussian distribution and complex t-distribution [41] will be revisited.

A Gaussian probabilistic model has been utilized to model the uncertainty of the FFT coefficients due to the added noise disturbance during the measurement process [53-55]. Gaussian probabilistic model states that, for the FFT random vector $\Psi_k = \left[F_i^{(\omega_k)}, Y_j^{(\omega_k)}\right]$ or $\Psi_k = \left[Y_i^{(\omega_k)}, Y_j^{(\omega_k)}\right]$, $\Psi_k^{\Re}$ and $\Psi_k^{\Im}$ are Gaussian distributed as the number of discrete-time points $N \to \infty$ according to the central limit theorem, and the PDF of the complex random vector Ψ_k is given by [55]:

$$p_{\boldsymbol{\Psi}_k}\left(\boldsymbol{\varphi}_k\right) = \frac{1}{\pi^{n_o}\left|\det \boldsymbol{\Sigma}_k\right|} e^{-\boldsymbol{\varphi}_k^* \boldsymbol{\Sigma}_k^{-1} \boldsymbol{\varphi}_k} \tag{28}$$

where $\boldsymbol{\varphi}_k$ denotes the value of the random vector $\boldsymbol{\Psi}_k$; the covariance matrix of $\boldsymbol{\Psi}_k$ is given by [55]:

$$\boldsymbol{\Sigma}_k = \mathbf{G}_k^{\Re} + \mathbf{i}\mathbf{G}_k^{\Im} \tag{29}$$

where $\mathbf{G}_k = E\left(\boldsymbol{\Psi}_k \boldsymbol{\Psi}_k^*\right)$ denotes the mathematical expectation of the raw PSD matrix of $\boldsymbol{\Psi}_k$.

Recent study reveals that the complex Gaussian distribution is tilted towards certain FFT coefficients, while complex-valued t-distribution offers a more viable alternative with respect to FFT coefficients at other frequencies, particularly because its peaks and tails are more realistic. Given that Ψ_k follows a complex-valued t-distribution, then the PDF is given by [41]:

$$p_{\boldsymbol{\Psi}_k}\left(\boldsymbol{\varphi}_k\right) = \frac{1}{\left(\pi/2\right)^{n_o} C\left(\vartheta, 2n_o\right)\left|\boldsymbol{\Xi}_k\right|}\left(1 + \frac{2}{\vartheta}\boldsymbol{\varphi}_k^* \boldsymbol{\Xi}_k^{-1} \boldsymbol{\varphi}_k\right)^{-(\vartheta+2n_o)/2} \tag{30}$$

where ϑ is the shape parameter of t-distribution, also known as the DOF of statistics; $\boldsymbol{\Xi}_k = \frac{\vartheta-2}{\vartheta}\boldsymbol{\Sigma}_k$.

4.3 Statistial inference for FRF and TF

In the context of statistical inference for FRF and TFs, the integral interval of the FFT coefficients are $[-\infty,+\infty]$. Therefore, the PDF of Z, the marginal PDF of $\mathrm{Z}^{\Re}$ and $\mathrm{Z}^{\Im}$, as well as the expected values of $\mathrm{Z}^{\Re}$ and $\mathrm{Z}^{\Im}$ are given by:

$$p_{\mathrm{Z}}(z) = \int_{-\infty}^{+\infty}\int_{-\infty}^{+\infty}|v|^2 p_{\Theta}(v\tilde{z})dv^{\Re}dv^{\Im} \tag{31a}$$

$$p_{\mathrm{Z}^{\Re}}(z^{\Re}) = \int_{-\infty}^{+\infty}\int_{-\infty}^{+\infty}\int_{-\infty}^{+\infty}|v|^2 p_{\Theta}(v\tilde{z})dv^{\Re}dv^{\Im}dz^{\Im} \tag{31b}$$

$$p_{\mathrm{Z}^{\Im}}(z^{\Im}) = \int_{-\infty}^{+\infty}\int_{-\infty}^{+\infty}\int_{-\infty}^{+\infty}|v|^2 p_{\Theta}(v\tilde{z})dv^{\Re}dv^{\Im}dz^{\Re} \tag{31c}$$

$$E(z^{\Re}) = \int_{-\infty}^{+\infty}\int_{-\infty}^{+\infty}\int_{-\infty}^{+\infty}\int_{-\infty}^{+\infty}|v|^2 p_{\Theta}(v\tilde{z})dv^{\Re}dv^{\Im}dz^{\Im}dz^{\Re} \tag{31d}$$

$$E(z^{\Im}) = \int_{-\infty}^{+\infty}\int_{-\infty}^{+\infty}\int_{-\infty}^{+\infty}\int_{-\infty}^{+\infty}|v|^2 p_{\Theta}(v\tilde{z})dv^{\Re}dv^{\Im}dz^{\Re}dz^{\Im} \tag{31e}$$

where $\tilde{\mathbf{z}} = \{1 \quad \mathbf{z}\}^T$.

Given the probabilistic models of $\Psi_k = \left[F_i^{(\omega_k)}, Y_j^{(\omega_k)}\right]$ and $\Psi_k = \left[Y_i^{(\omega_k)}, Y_j^{(\omega_k)}\right]$, we can determine the PDF of FRF and TF using Eq.(31) by replacing the general mathematical symbols as follows:

- For FRF: $\Theta = \Psi_k = \left[F_i^{(\omega_k)}, Y_j^{(\omega_k)}\right]$; $\mathrm{Z} = H_{ij}^{(\omega_k)}$; $\tilde{\mathrm{Z}} = \left[1, H_{ij}^{(\omega_k)}\right]^T$; $V = F_i^{(\omega_k)}$; $V\tilde{\mathrm{Z}} = F_i^{(\omega_k)}\left[1, H_{ij}^{(\omega_k)}\right]$.
- For TF: $\Theta = \Psi_k = \left[Y_i^{(\omega_k)}, Y_j^{(\omega_k)}\right]$; $\mathrm{Z} = T_{ij}^{(\omega_k)}$; $\tilde{\mathrm{Z}} = \left[1, T_{ij}^{(\omega_k)}\right]^T$; $V = Y_i^{(\omega_k)}$; $V\tilde{\mathrm{Z}} = Y_i^{(\omega_k)}\left[1, T_{ij}^{(\omega_k)}\right]$.

As a result, we can use the SGQ rule introduced in Section 3 to solve the PDF of Z as well as its extensions. The procedures for computing the PDF for FRFs are summarized in Table 4, which can be easily extended to the case of TF.

Algorithm 4: Statistical inference for FRF using the unified scheme

Step	Procedures
1	Take FFT for different sets of time histories $\Psi_k = \left[F_i^{(\omega_k)}, Y_j^{(\omega_k)}\right]$;
2	Calculate the covariance of the FFT samples of different measurements $\boldsymbol{\Sigma}_k = \mathbf{G}_k^{\Re} + \mathbf{i}\mathbf{G}_k^{\Im}$ with $\mathbf{G}_k = E\left(\boldsymbol{\Psi}_k \boldsymbol{\Psi}_k^*\right)$;
3	FOR $k = k_1 : k_2$ ● Select the probabilistic model for FFT coefficients $p_{\boldsymbol{\Psi}_k}\left(\boldsymbol{\varphi}_k\right)$ at ω_k; ● Formulate $p_\Theta\left(v\tilde{z}\right)$ by setting $\Theta = \Psi_k = \left[F_i^{(\omega_k)}, Y_j^{(\omega_k)}\right]$, $\mathrm{Z} = H_{ij}^{(\omega_k)}$, $\tilde{\mathrm{Z}} = \left[1, H_{ij}^{(\omega_k)}\right]^T$, $V = F_i^{(\omega_k)}$ and $V\tilde{\mathrm{Z}} = F_i^{(\omega_k)}\left[1, H_{ij}^{(\omega_k)}\right]$. ● Formulate the unified formula by substituting $p_\Theta\left(v\tilde{z}\right)$ into (31); ● Generate SGQ points and weights for $V^{\Re}$, $V^{\Im}$, $\mathrm{Z}^{\Re}$ and $\mathrm{Z}^{\Im}$ by following Table 1; ● Calculate multiple integrals in Eq. (31) following the Table 3. END FOR

5 Case Studies

5.1 Vibration testing of a simply-supported beam

To illustrate the efficiency of the proposed methodology of this study, the theoretical findings are validated with tests on a simply-supported beam shown in Fig. 2. The length of the beam is 3 meters, while its cross section is $0.1m \times 0.02m$. The beam was subject to hammer excitation. The input force and output acceleration were measured simultaneously with the sampling frequency of $200Hz$. To verify the proposed probabilistic models, the response measurements are segmented into 360 non-overlapping sequences with each one lasting 300 s. The FFT coefficients were then calculated for each realization to formulate samples of the FRFs and TFs at different ω_k. As a result, a thorough validation can be implemented in a similar way to MCS with each segment viewed as a random realization.

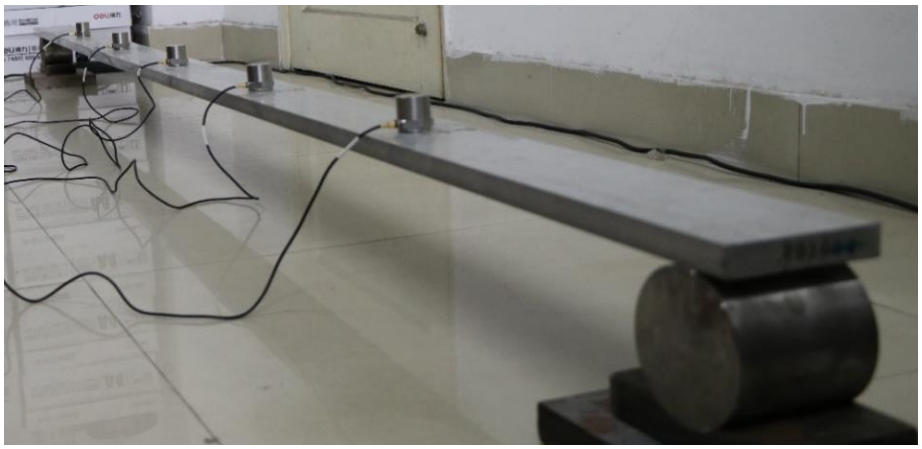

Fig. 2: The tested simply-supported beam

5.1.1 The K-S test of FFT coefficients

The K-S test was conducted by comparing the distribution of the samples (i.e., the FFT coefficients) with an assumed distribution for the real and the imaginary parts within the frequency band [0,10] Hz. When the K-S test is equal to 0, the FFT coefficients follow the assumed distribution; when K-S test is equal to 1, the corresponding probability model and the assumption should be rejected. The K-S test by assuming that the real and imaginary parts of FFT coefficients of $F_1^{(\omega_k)}$ and $Y_1^{(\omega_k)}$ follow Gaussian distribution are shown in Fig. 3(a) and 3(b), which indicate that the complex Gaussian distribution can model the distributions of FFT coefficients at a set of frequencies successfully. However, the test data analysis also emphasizes the existence of non-Gaussianity, especially for the excitation. The K-S test by assuming that the real and imaginary parts of FFT coefficients of $F_1^{(\omega_k)}$ and $Y_1^{(\omega_k)}$ follow t-distribution are shown in Fig. 4(a) and 4(b). By comparing Fig.3 and Fig.4, the passing rates of the t-distribution are significantly higher than that of the Gaussian distribution. Therefore, complex Gaussian probabilistic model and complex t probabilistic model will be used to model FFT coefficients at different frequencies, which will be further used to infer the statistical distribution of FRF and TF.

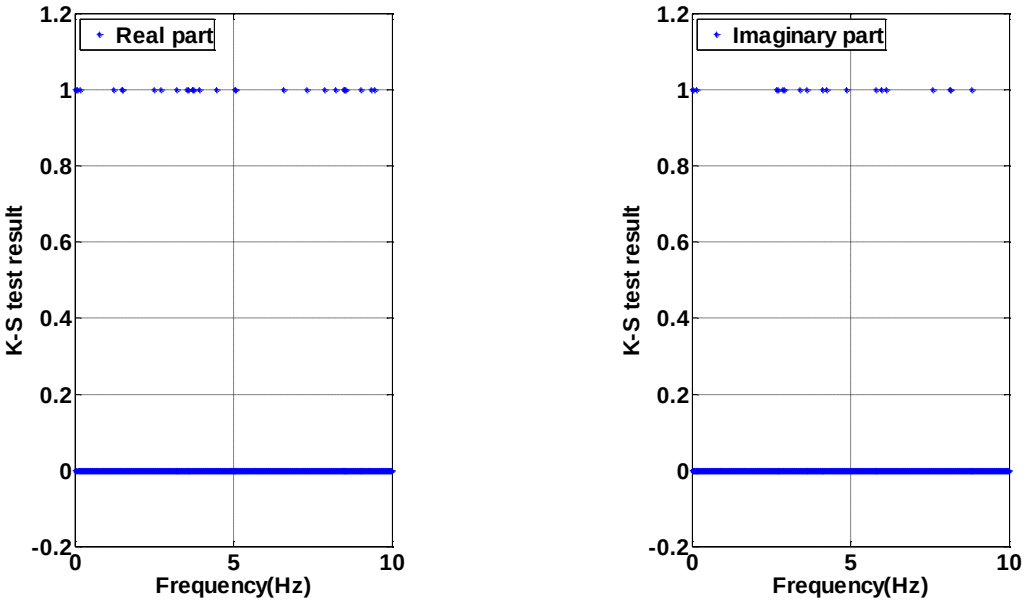

(a) The real (left) and imaginary parts (right) of $F_1^{(\omega_k)}$

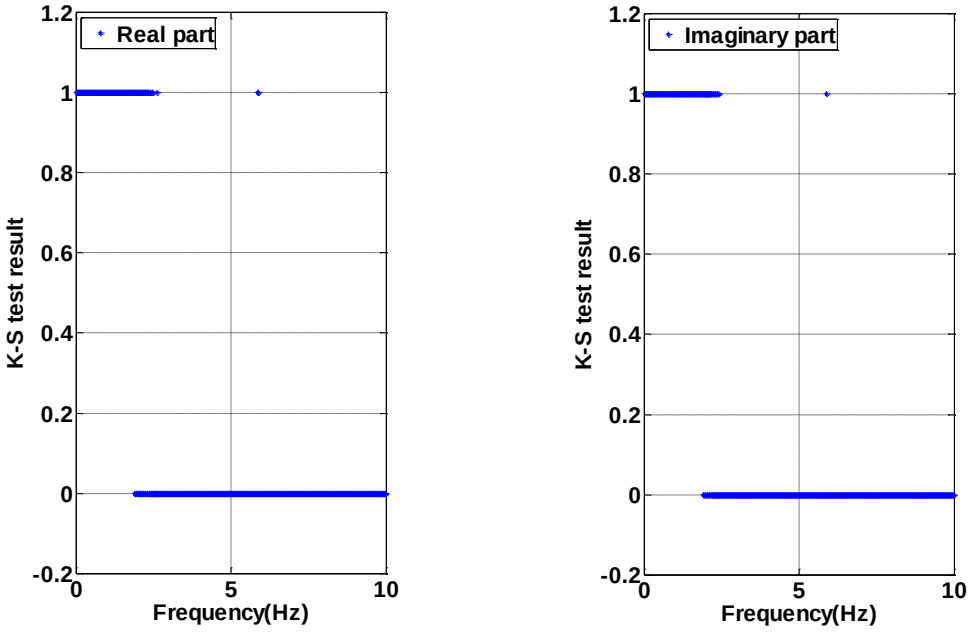

(b) The real (left) and imaginary part (right) of $Y_1^{(\omega_k)}$

Fig.3: K-S test of the real and imaginary parts of FFT coefficients of $F_1^{(\omega_k)}$ and $Y_1^{(\omega_k)}$ by comparing the distribution of the samples with the Gaussian distribution

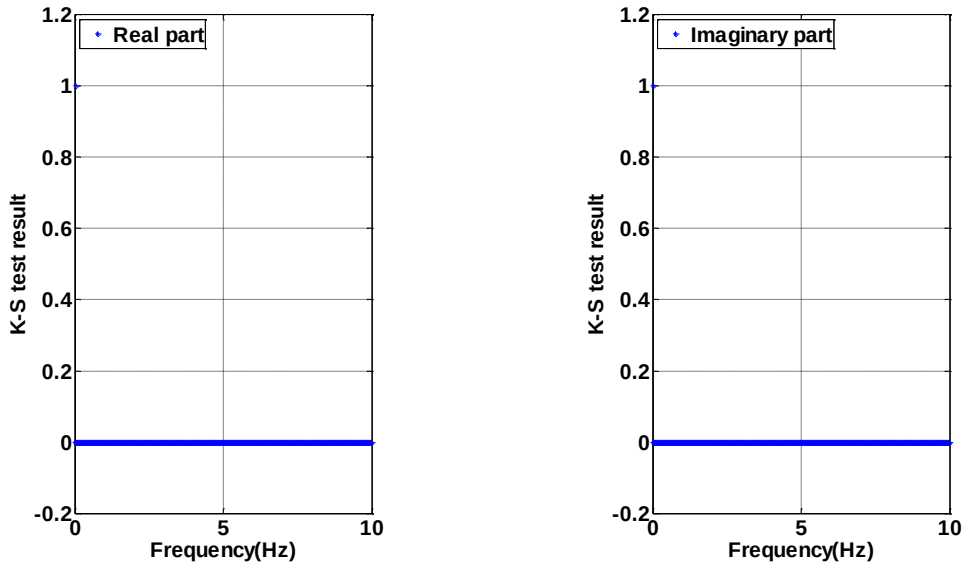

(a) The real (left) and imaginary part (right) of $F_1^{(\omega_k)}$

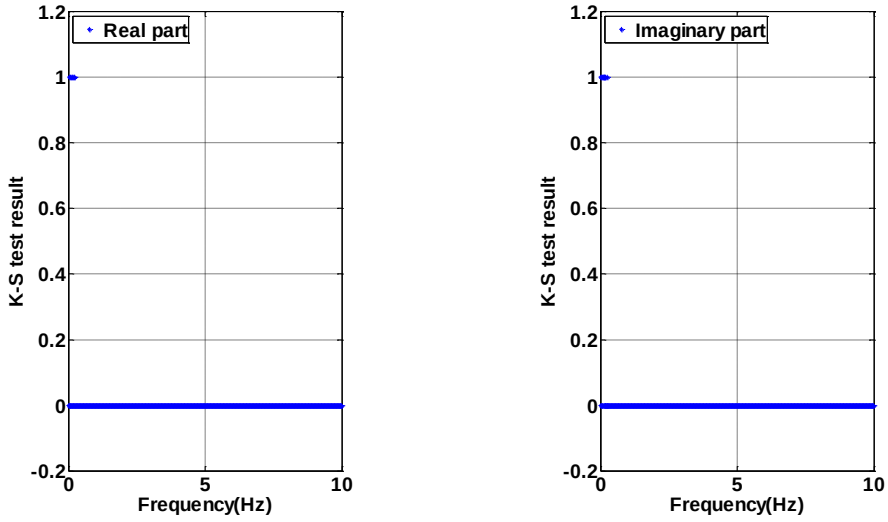

(b) The real (left) and imaginary part (right) of $Y_1^{(\omega_k)}$

Fig.4: K-S test of the real and imaginary parts of FFT coefficients of $F_1^{(\omega_k)}$ and $Y_1^{(\omega_k)}$ by comparing the distribution of the samples with the t-distribution

5.1.2 Statistical inference for FRFs

The distribution properties of the FRF $H_{15}^{(\omega_k)}$ at $\omega_k = 8.28\pi \text{ rad/s}$, which passes the K-S test, were observed. At the frequency line $\omega_k = 8.28\pi \text{ rad/s}$, the K-S test shows that it follows

Gaussian distribution. Here the FRF can be modelled by univariate circularly-symmetric complex Gaussian ratio distribution whose closed-form formula has been derived in [21]. By denoting covariance matrix of $\left[F_1^{(\omega_k)}, Y_5^{(\omega_k)}\right]$ as $\mathbf{\Sigma} = \begin{bmatrix} \sigma_0^2 & \rho\sigma_0\sigma_1 \\ \rho^*\sigma_0\sigma_1 & \sigma_1^2 \end{bmatrix}$ where $\rho = \rho^{\Re} + \mathbf{i}\rho^{\Im}$ denotes the complex correlation coefficient, the analytical formula of $p_Z(z)$, $p_{Z^{\Re}}(z^{\Re})$ and $p_{Z^{\Im}}(z^{\Im})$ are given by:

$$p_Z(z) = \pi^{-1}(1-\rho^*\rho)\sigma_0^2\sigma_1^2\left[\sigma_1^2 - (z^*\rho^* + z\rho)\sigma_0\sigma_1 + zz^*\sigma_0^2\right]^{-2} \tag{32a}$$

$$p_{Z^{\Re}}(z^{\Re}) = \frac{(1-|\rho|^2)\sigma_0^4\sigma_1^2}{2\sqrt{[-2\sigma_0^3\sigma_1\rho^{\Re}z^{\Re} + \sigma_0^4(z^{\Re})^2 + \sigma_0^2\sigma_1^2(1-(\rho^{\Im})^2)]^3}} \tag{32b}$$

$$p_{Z^{\Im}}(z^{\Im}) = \frac{(1-|\rho|^2)\sigma_0^4\sigma_1^2}{2\sqrt{(2\sigma_0^3\sigma_1\rho^{\Im}z^{\Im} + \sigma_0^4(z^{\Im})^2 + \sigma_0^2\sigma_1^2(1-(\rho^{\Re})^2))^3}} \tag{32c}$$

Fig. 5 compares the theoretical curves of the real and imaginary parts of $H_{15}^{(\omega_k)}$ (i.e., Eq.(32b) and (32c)), denoted by dotted lines, with the probability mass functions represented by histograms drawn from all the samples. For the purpose of comparison, the PDF of $H_{15}^{(\omega_k)}$ was also calculated by using the SGQ algorithm introduced in Section 3 and plotted in Fig. 5 by solid lines. As is seen in Fig. 5, the curve achieved by using the numerical algorithm coincide with the closed-from formula (32), both of which can fit the histograms well. Therefore, the unified scheme to solving the complex-valued ratio distribution can achieve satisfactory results.

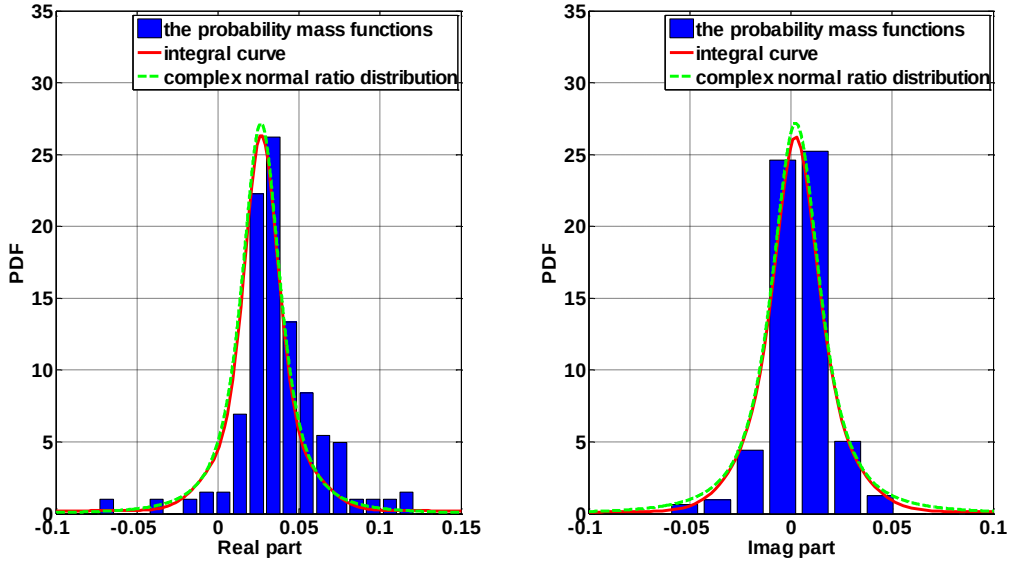

Fig.5: Comparison of the marginal PDFs calculated using the analytical formula (Eq.(32)) and numerical method as well as the histogram of the real part and imaginary part of $H_{15}^{(\omega_k)}$ at $\omega_k = 8.28\pi$ rad/ s .

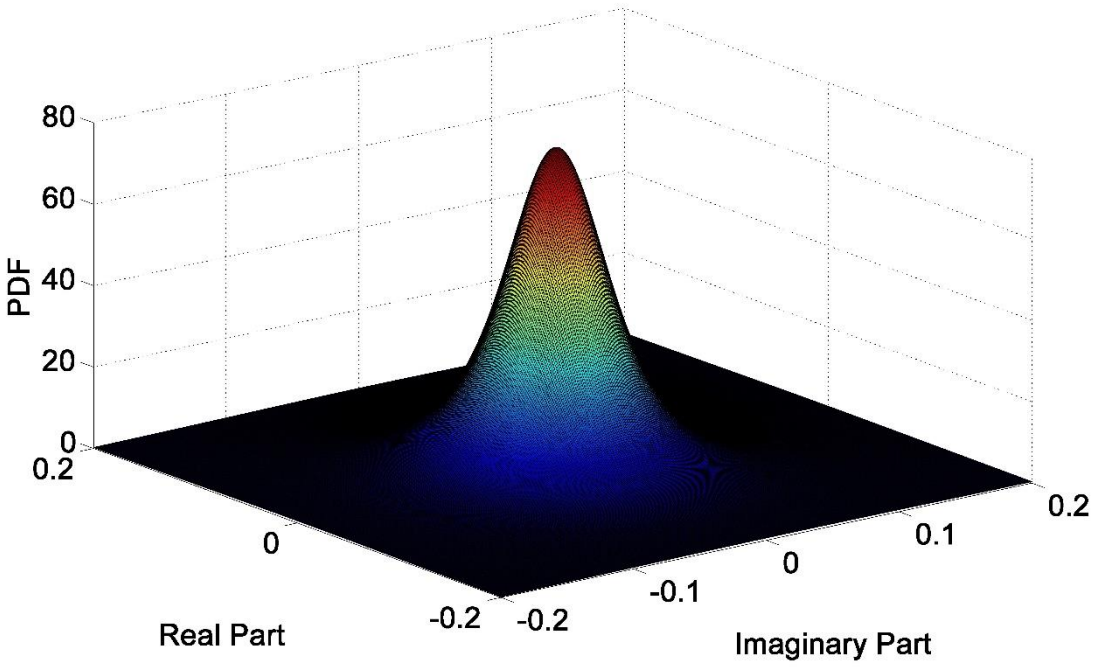

Fig. 6: The 3-D shaded surface plot of the joint PDF of the real and imaginary parts of $H_{15}^{(\omega_k)}$ at $\omega_k = 0.18\pi$rad/ s

To further illustrate the efficiency of the unified approach, the distribution properties of $H_{15}^{(\omega_k)}$ at $\omega_k = 0.18\pi \text{rad/s}$, which pass the K-S test of t-distribution, were also observed. The variance of $F_1^{(\omega_k)}$ and $Y_5^{(\omega_k)}$ are equal to 0.0679 and 0.0062, respectively, while their complex correlation coefficient is equal to 0.1907-0.0228i. For $F_1^{(\omega_k)}$ and $Y_5^{(\omega_k)}$, the shape parameters of t-distribution are set as 9 and 3. The random variable $H_{15}^{(\omega_k)}$ at $\omega_k = 0.18\pi \text{rad/s}$ is modelled using complex t ratio distribution, whose PDF was computed by following the procedures in Table 4. Fig. 6 shows the 3-D shaded surface plot of the joint PDF of the real and imaginary parts of $H_{15}^{(\omega_k)}$ at $\omega_k = 0.18\pi \text{rad/s}$. In Fig. 7, the solid line and the dotted line denote the PDFs of $H_{15}^{(\omega_k)}$ at $\omega_k = 0.18\pi \text{rad/s}$ computed with the proposed numerical algorithm and those of circularly-symmetric complex Gaussian ratio distribution, respectively, while the histograms denote the probability mass functions achieved from the FFT samples. The comparison shown in Fig.7 indicates that the t ratio distribution can be computed with high accuracy using the numerical algorithm, and its performance is much better than that of complex Gaussian distribution at some frequency points.

Table 5 shows the time consumption of computing the PDF of $H_{15}^{(\omega_k)}$, the marginal PDF of $\left[H_{15}^{(\omega_k)}\right]^{\Re}$ and the mean of $\left[H_{15}^{(\omega_k)}\right]^{\Re}$ at $\omega_k = 0.18\pi \text{rad/s}$ by using Gaussian quadrature rule and SGQ rule introduced in Section 3. From Table 5, one can figure out that the time consumed by the proposed numerical scheme of employing sparse-grid theory is reduced significantly. Therefore, the unified solution is expected to be efficient in quantifying the uncertainties of FRF when it is highly non-trivial to obtain its closed-form solution due to the complexity of multidimensional integrals.

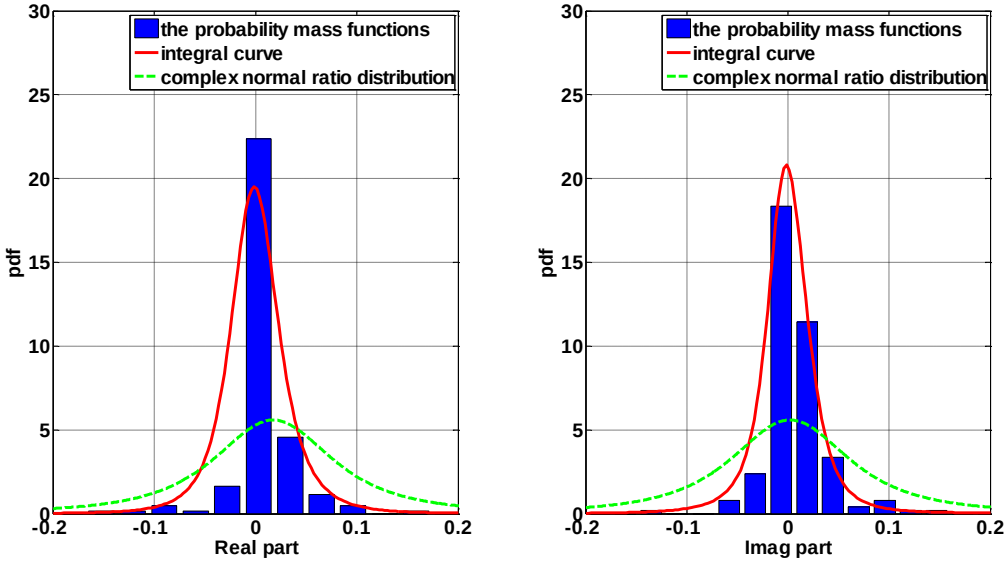

Fig.7: The marginal PDFs and the histogram of the real part and imaginary part of $H_{15}^{(\omega_k)}$ at $\omega_k = 0.18\pi \text{rad/s}$: the complex t ratio distribution computed with the SGQ rule is denoted by solid line while the complex Gaussian ratio distribution is denoted by dotted line.

Table 5: Time consumed by two different numerical strategies for the simply-supported beam

Items	PDFs	Time (s)	
		Gaussian quadrature	Sparse-grid quadrature
FRF at $\omega_k = 0.18\pi \text{rad/s}$	PDF of $H_{15}^{(\omega_k)}$	62.87	6.85
	Marginal PDF of $\left[H_{15}^{(\omega_k)}\right]^{\Re}$	493.04	18.11
	Expectation of $\left[H_{15}^{(\omega_k)}\right]^{\Re}$	7086.75	19.35
TF at $\omega_k = 4.31\pi \text{rad/s}$	PDF of $T_{15}^{(\omega_k)}$	65.72	7.16
	Marginal PDF of $\left(T_{15}^{(\omega_k)}\right)^{\Re}$	486.23	17.86
	Expectation of $\left(T_{15}^{(\omega_k)}\right)^{\Re}$	6368.92	17.39

5.1.3 Statistical inference for TFs

To illustrate the applicability of the proposed unified solution of complex ratio distribution, the performance of TFs are observed in this part. The TF corresponding to the fifth sensor and the first sensor (i.e., $T_{15}^{(\omega_k)}$) is considered first at the frequency line $\omega_k = 4.31\pi rad/s$. The variance of $Y_1^{(\omega_k)}$ and $Y_5^{(\omega_k)}$ are equal to 7.3587×10^{-5} and 7.6863×10^{-5}, respectively, and their complex correlation coefficient is equal to $0.7047+0.0244i$. The K-S test result indicates that $T_{15}^{(\omega_k)}$ at $\omega_k = 4.31\pi \text{rad/s}$ follows complex t ratio distribution. The shape parameters of $Y_1^{(\omega_k)}$ and $Y_5^{(\omega_k)}$ are set to be 5. Following the procedures demonstrated in Table 4, the unified formula of the PDF of $T_{15}^{(\omega_k)}$ can be determined according to Eq. (31), which was then solved numerically by using the SGQ rule introduced in Section 3. The 3-D shaded surface plot of the joint PDF of the real and imaginary parts of $T_{15}^{(\omega_k)}$ presented in Fig. 8.

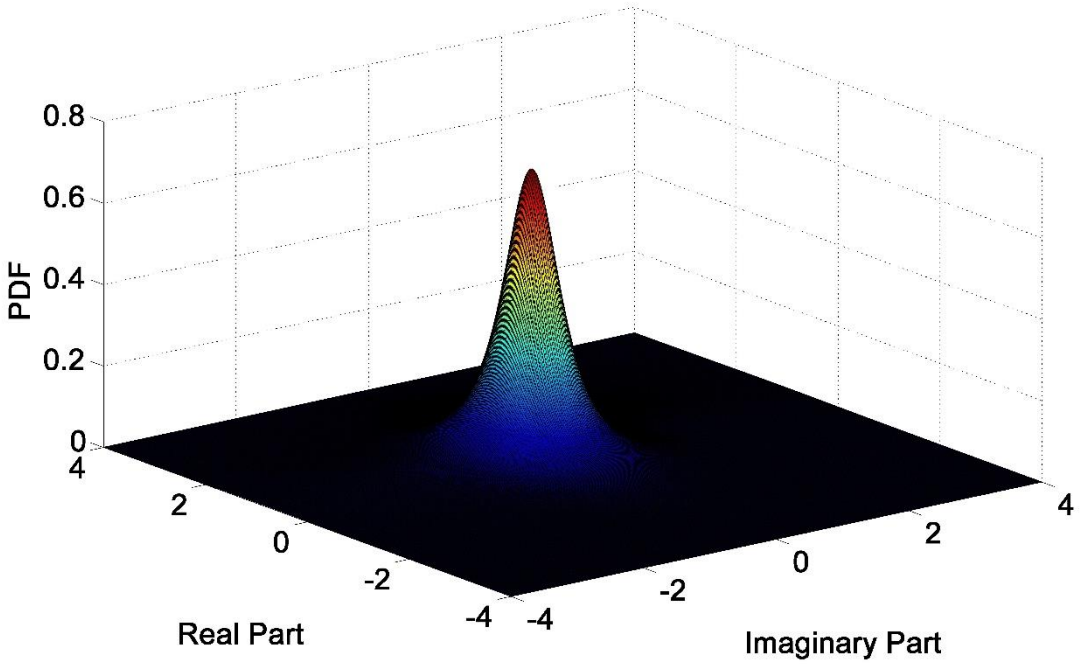

Fig. 8: The 3-D shaded surface plot of the joint PDF of the real and imaginary parts of $T_{15}^{(\omega_k)}$ at $\omega_k = 4.31\pi \text{rad/s}$

In Fig.9, the solid line denotes the PDFs of the real and imaginary parts of $T_{15}^{(\omega_k)}$, while the histograms denote the probability mass functions drawn from 360 samples. As is seen from Fig.9, there is a good consistency between the observed histograms and the PDF of complex t ratio distribution which was calculated using the SGQ rule. The time required for computing the PDF of $T_{15}^{(\omega_k)}$, marginal PDF of $\left[T_{15}^{(\omega_k)}\right]^{\Re}$, as well as the expected value of $\left[T_{15}^{(\omega_k)}\right]^{\Re}$ at $\omega_k = 4.31\pi$ rad/ s by Gaussian quadrature rule and SGQ rule are also compared in Table 5, which clearly demonstrates again that the unified formula of complex ratio distribution shown in Eq.(31) can be computed using SGQ rule more efficiently than conventional multidimensional Gaussian quadrature rule when the analytical formula is not available.

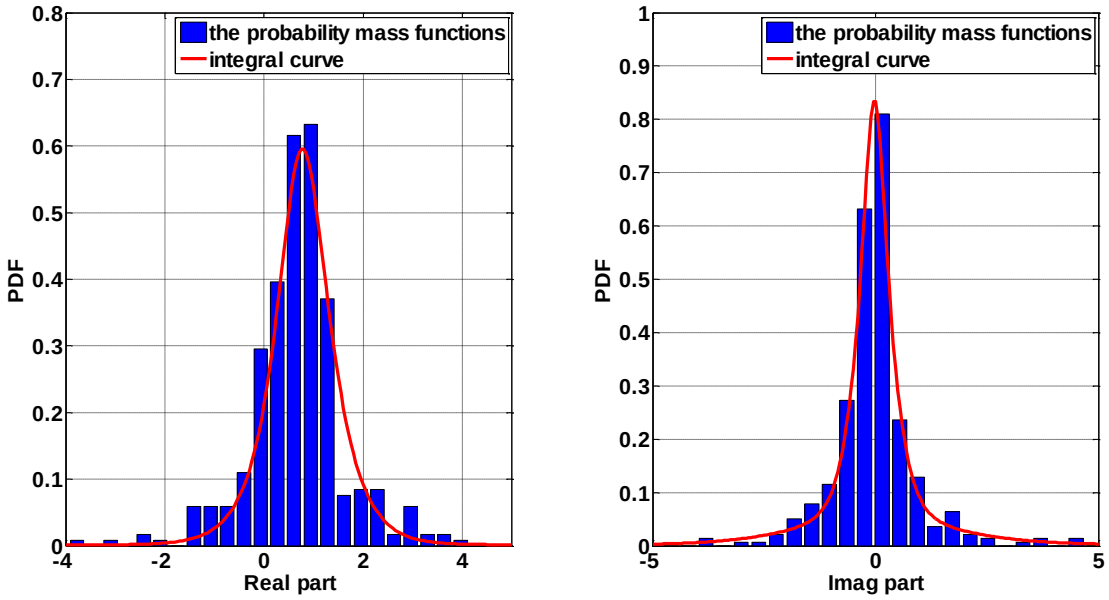

Fig. 9: The marginal PDFs and the histogram of the real part and imaginary part of $T_{15}^{(\omega_k)}$ at $\omega_k = 4.31\pi$ rad/ s

5.2 Performance evaluation using the test of Alamosa Canyon Bridge

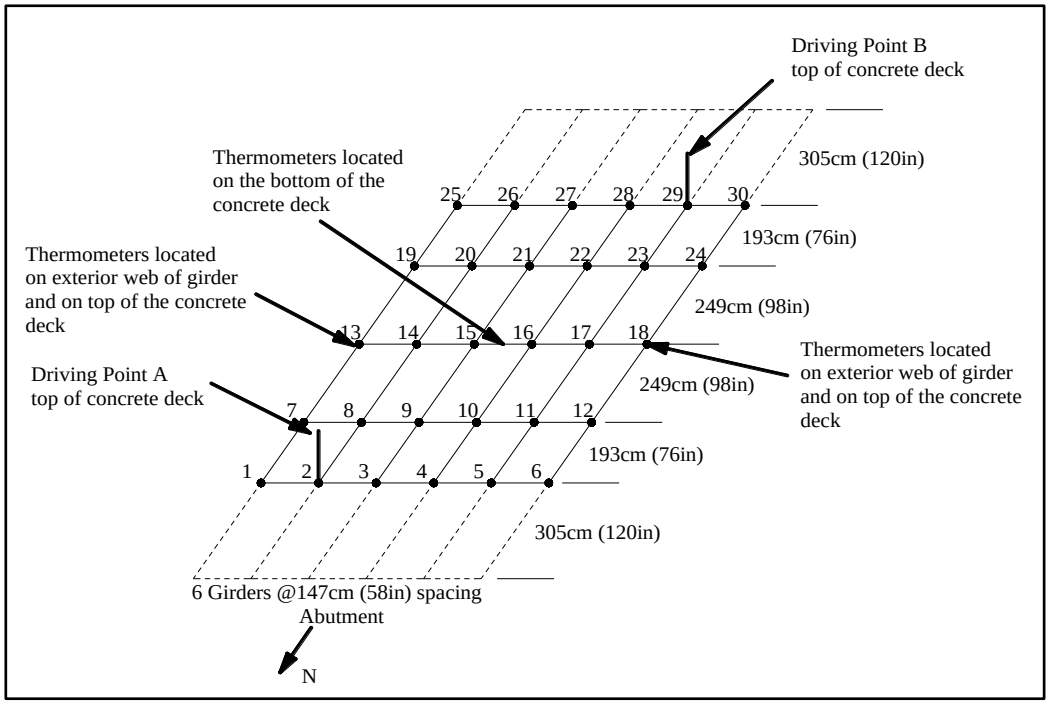

Fig.10: Positions of the accelerometer of the Alamosa Canyon Bridge (from [58])

This section will further evaluate the performance of the unified solution of computing the complex ratio distribution by using the field test measurement of the Alamosa Canyon Bridge. This bridge is located approximately 16 km north of Truth or Consequences, New Mexico [58]. The bridge has seven independent spans with each span consisting of a concrete deck supported by six steel beams. The roadway in each span is approximately 7.3 m wide and 15.2 m long. Expansion joints are located at both ends of each span. The concrete deck and the girders below the bridge were equipped with a total of 31 acceleration measurements as shown in Fig. 10.

This field test of the bridge was conducted on the Bridge to study various issues related to bridge structural integrity. Due to the efforts of the researchers from the Los Alamos National Laboratory, a website (http://ext.lanl.gov/projects/damage_id/) has been established for collecting various vibration test data as a benchmark problem. The field test data used in this

study last 24 hours, ranging from July 21, 1997 to July 23, 1997. The sampling rate of the acceleration data is 128 Hz.

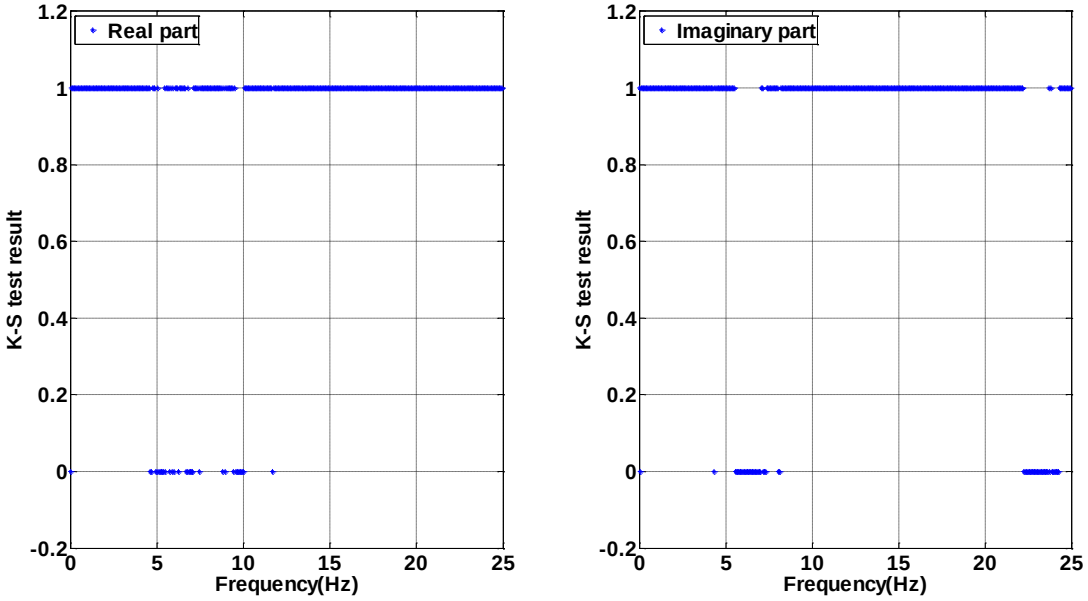

(a) The Gaussian distribution

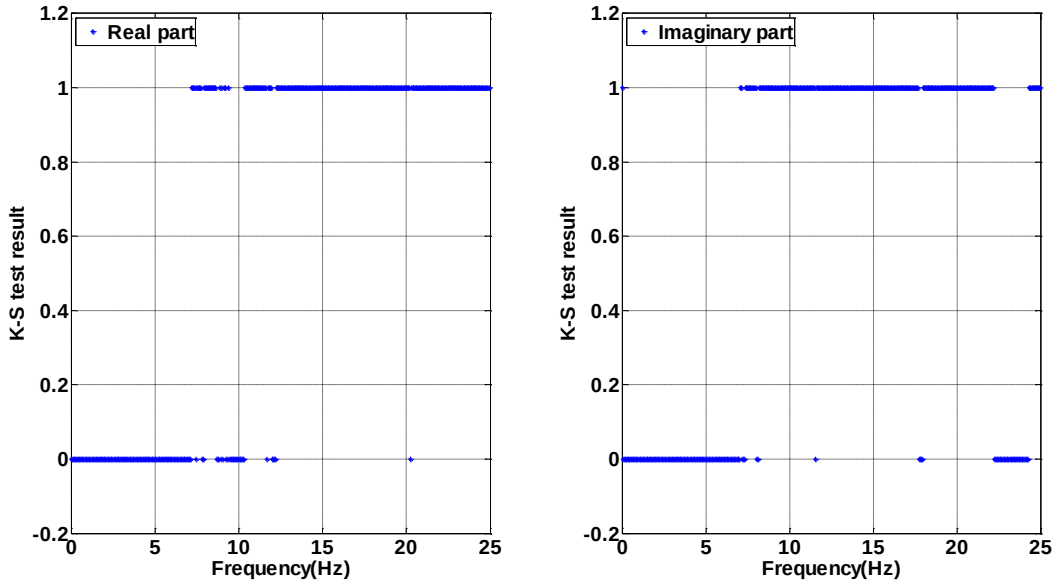

(b) The t-location scale distribution

Fig.11. K-S test of the real part and imaginary parts of FFT coefficients of $Y_1^{(\omega_k)}$ by assuming two different-distributions

The response measurements are segmented into 330 non-overlapping sequences with each one lasting 16 s. The FFT coefficients can be calculated accordingly for each sequence. Like MCS, each segment can be viewed as a random realization and one can employed to draw the histograms to validate the accuracy of the theoretical PDF. By analyzing the measurements acquired from different sensors, the following analyses were conducted:

- The K-S test was conducted by comparing the distribution of the samples (i.e., the FFT coefficients) with the Gaussian distribution and t-distribution for the real and imaginary parts of the FFT coefficients of the first channel $Y_1^{(\omega_k)}$ within the frequency band 0-25 Hz, and the significance level was set to 0.05. The results are shown in Fig. 11. For the FFT coefficients at a number of frequencies, the results of the K-S test suggest that the complex Gaussian probability model could not adequately capture the statistics of all samples while the *t*-distribution can model FFT coefficients well at a number of frequencies well.

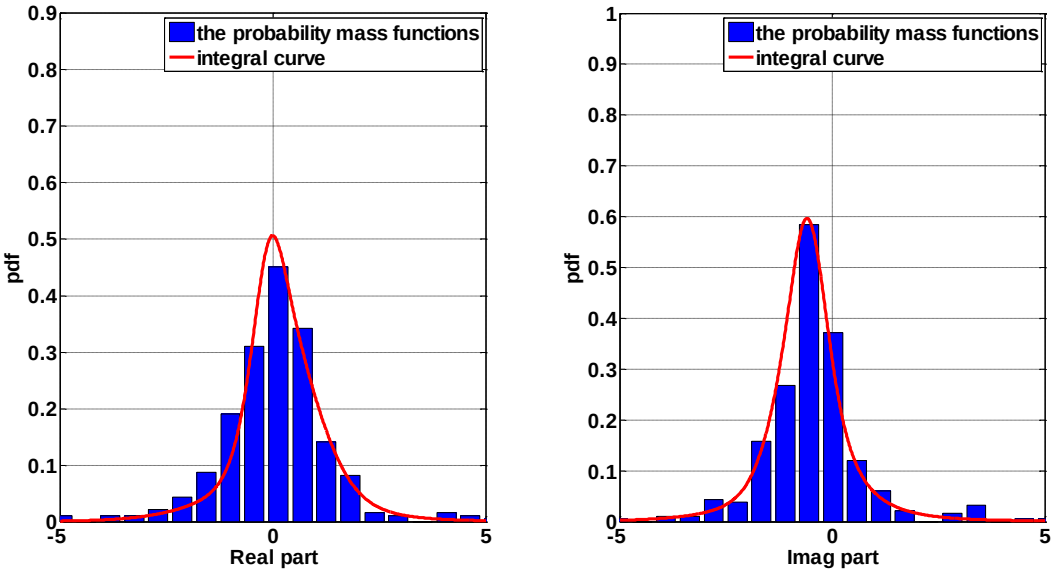

Fig.12: The theoretical marginal PDFs and the histograms of the real and imaginary parts of $H_{31}^{(\omega_k)}$ at $\omega_k = 6.875\pi \text{rad/s}$

- The real and imaginary parts of FFT coefficient samples $F_3^{(\omega_k)}$ and $Y_1^{(\omega_k)}$ at $\omega_k = 6.875\pi \text{rad/s}$ can be well fitted by t-distribution. The variances of $F_3^{(\omega_k)}$ and $Y_1^{(\omega_k)}$

are 4.925×10^{-5} and 5.410×10^{-5}, and their complex correlation coefficient is $0.1233+0.2384\mathrm{i}$. Therefore, $H_{31}^{(\omega_k)}$ at $\omega_k = 6.875\pi \mathrm{rad/s}$ can be modelled using complex-valued t ratio distribution. Fig. 12 compares the theoretical curves of the real and imaginary parts of $H_{31}^{(\omega_k)}$ at $\omega_k = 6.875\pi \mathrm{rad/s}$ denoted by solid lines with the probability mass functions denoted by histograms drawn from all samples. Fig. 12 shows that the solid curves (i.e., Eq.(31)) obtained by numerical integration agree with the histograms, indicating that it is common for the FRFs to follow complex non-Gaussian ratio distribution whose closed-form is difficult to be achieved.

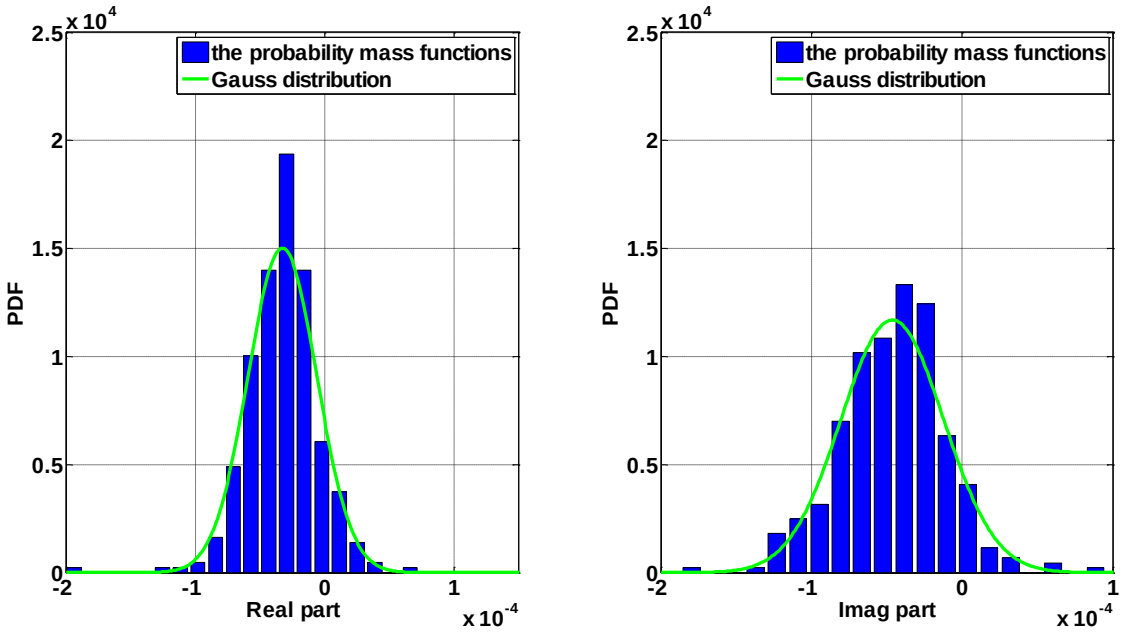

(a) $Y_1^{(\omega_k)}$ at $\omega_k = 11.5\pi \mathrm{rad/s}$

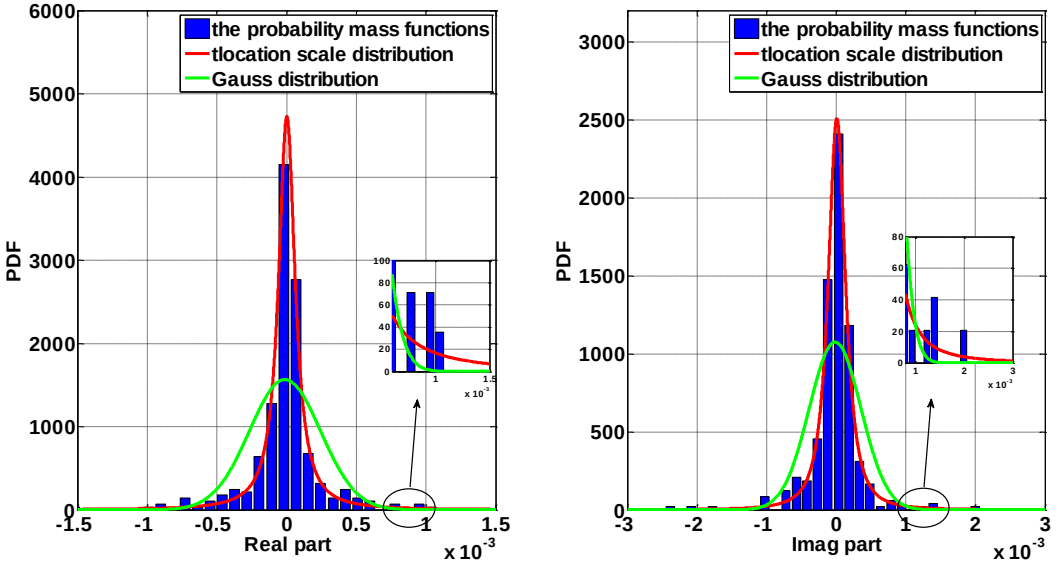

(b) $Y_1^{(\omega_k)}$ at $\omega_k = 1.25\pi\, rad/\, s$

Fig.13: The theoretical marginal PDFs and the histogram of the real and imaginary part of $Y_1^{(\omega_k)}$ at $\omega_k = 11.5\pi$ rad/ s and $\omega_k = 1.25\pi\, rad/\, s$

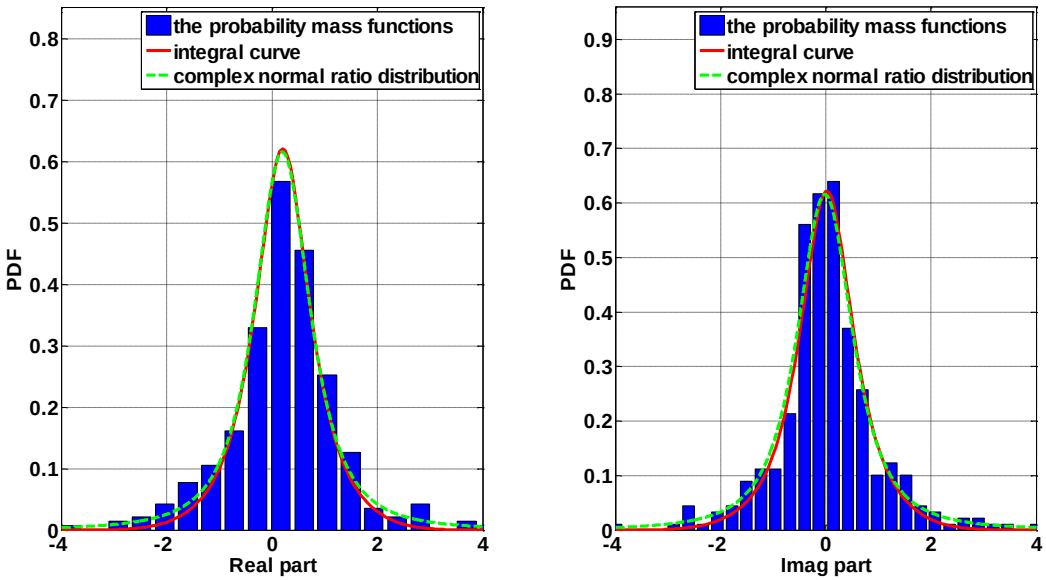

(a) $T_{11,1}^{(\omega_k)}$ at $\omega_k = 11.5\pi$ rad/ s

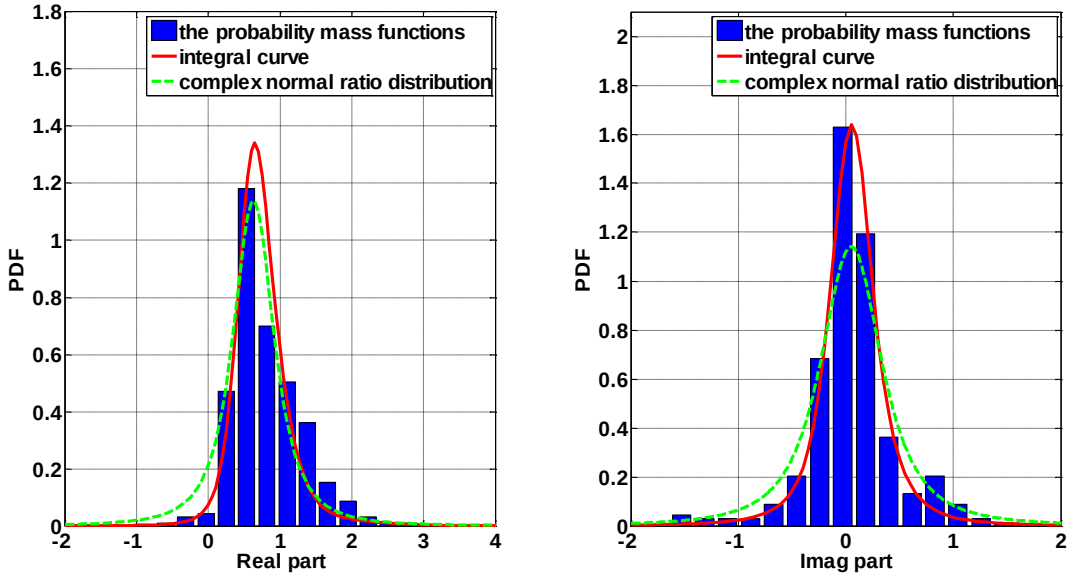

(b) $T_{11,1}^{(\omega_k)}$ at $\omega_k = 1.25\pi\, rad/\ s$

Fig.14: The theoretical marginal PDFs and the histogram PDFs of the real part and imaginary part of $T_{11,1}^{(\omega_k)}$ at $\omega_k = 11.5\pi$ rad/ s and $\omega_k = 1.25\pi\, rad/\ s$

- The TF $T_{11,1}^{(\omega_k)}$ corresponding to the eleventh sensor and the first sensor $\omega_k = 11.5\pi$ rad/ s and $\omega_k = 1.25\pi\, rad/\ s$ are also observed in detail. The real and imaginary parts of $Y_{11}^{(\omega_k)}$ at $\omega_k = 11.5\pi$ rad/ s and $\omega_k = 1.25\pi\, rad/\ s$ are shown in Fig.13(a) and Fig. 13(b), respectively. In Fig.14(a), the solid line denotes the complex Gaussian ratio distribution computed with SQG rule, while the dotted lines are plot according to the closed-from formula of complex Gaussian ratio distribution. In Fig. 14(b), the solid line denotes the complex t ratio distribution achieved by using the unified formula solved with SQG rule while the dotted lines denote the analytical formula of complex Gaussian ratio distribution. Both Fig. 14(a) and 14(b) are accompanied by the histograms denoting the probability mass functions of 330 samples. As is seen from Fig.14(a), there is a good consistency between

the observed histograms, the curves of the analytical values and the numerical values for both the real and imaginary parts. In Fig.14(b), the t ratio distribution is a better candidate for modeling $T_{11,1}^{(\omega_k)}$ at $\omega_k = 1.25\pi\, rad/\,s$. Furthermore, both Fig.14(a) and 14(b) verify that, given the accurate probabilistic model of FFT coefficients, the PDF of the TFs can be solved by using the numerical algorithm efficiently.

- The time required for computing the PDF of $H_{3,1}^{(\omega_k)}$ and $T_{11,1}^{(\omega_k)}$, marginal PDF of $\left[H_{3,1}^{(\omega_k)}\right]^{\Re}$ and $\left[T_{11,1}^{(\omega_k)}\right]^{\Re}$, as well as the expected value of $\left[H_{3,1}^{(\omega_k)}\right]^{\Re}$ and $\left[T_{11,1}^{(\omega_k)}\right]^{\Re}$ at $\omega_k = 6.875\pi \text{rad/ s}$ and $\omega_k = 1.25\pi\, rad/\,s$ by Gaussian quadrature rule and SGQ rule are compared in Table 6. From Table 6, one can figure out that the time consumed by sparse-grid quadrature rule is significantly less than those of classic Gaussian quadrature rule since much less Gaussian points are involved. Therefore, the unified solution is expected to be efficient in quantifying the uncertainties of FRFs and TFs by integrating the unified formula of complex ratio distribution with multidimensional integrals and the SGQ rule when it is difficult to find the closed-form solution.

Table 6: Time consumed by two different numerical strategies for the Alamosa Canyon Bridge

Items	PDFs	Time (s)	
		Gaussian quadrature	Sparse-grid quadrature
FRF at $\omega_k = 6.875\pi \text{rad/ s}$	PDF of $H_{3,1}^{(\omega_k)}$	73.61	8.02
	Marginal PDF of $\left[H_{3,1}^{(\omega_k)}\right]^{\Re}$	515.09	18.93
	Expectation of $\left[H_{3,1}^{(\omega_k)}\right]^{\Re}$	7277.20	19.87
TF at $\omega_k = 1.25\pi\, rad/\,s$	PDF of $T_{11,1}^{(\omega_k)}$	67.28	7.33
	Marginal PDF of $\left[T_{11,1}^{(\omega_k)}\right]^{\Re}$	514.82	18.91

	Expectation of $\left[T_{11,1}^{(\omega_k)}\right]^{\mathfrak{R}}$	7064.78	19.29

6 Conclusions

In engineering science, complex-valued ratio functions arise within several fields. It has been recognized that it is of significant value to quantify uncertainty by employing the PDF which holds the most fundamental role in extracting the useful statistical information from available data. This paper derives a unified formula for arbitrary complex ratio random variables based on the principle of probability transformation in the complex domain. The general solution is obtained by an efficient numerical integral method. To address the drawbacks of multidimensional Gaussian quadrature formulas, a fast quadrature approach based on the sparse-grid theory was employed to address the curse of dimensionality problem. The locations and weights of the univariate quadrature points with a range of accuracy levels are determined by an asymptotic approximation method. Then the univariate quadrature point sets are extended to form a multi-dimensional grid using the sparse-grid theory. The method proposed can tackle various ratio distributions, such as Gaussian or non-Gaussian, correlated or independent, bounded or unbounded ratio random variables.

The unified scheme to solve complex ratio distribution was then applied to statistical inference for FRFs and TFs which are important tools in a vast range of applications including modal analysis and damage detection. The classic complex Gaussian ratio distribution whose analytical PDF has been derived recently is being increasingly used to model the distributions of FRFs and TFs due to its elegant and convenient mathematical nature. However, the field-test data analysis for engineering structures emphasizes the possibility of non-Gaussianity for some FFT observations due to various reasons such as nonstationarity of the data, the limited length of the data available, etc. Given that the FFT coefficients follow complex non-Gaussian

distribution, it is difficult to derive the closed-formula for complex ratio distributions, and thus the unified scheme proposed in this study offers a good alternative.

The theoretical findings of this study are verified using response measurements of a simply supported beam and the Alamosa Canyon bridge. Discrepancies between the analytical PDFs and corresponding histograms are plotted to display the accuracy of the probabilistic models. It is worth mentioning here that, the histogram of FRF and TF samples can be well predicted by the theoretical PDFs given that we can model the FFT samples well by a proper complex-valued probabilistic model. The time required for computing the PDF, the marginal PDF as well as the expectation of complex ratio distribution by Gaussian quadrature rule and SGQ rule are also compared to highlight the efficiency of the SGQ rule. Results indicate that the unified computational probability model incorporating an SGQ numerical algorithm proposed in this study can quantify the uncertainty of complex ratio random variables much more efficiently. This study yields new insights into the qualitative analysis of the uncertainty of FRFs and TFs, which paves the way for developing new statistical methodologies for modal analysis, model updating or damage detection using structural responses.

Acknowledgement

Financial support to complete this study was provided in part by Natural Science Foundation of China (No. 51778203 and 51778204). The authors would thank Los Alamos National Laboratory for providing the data from the various vibration tests performed on the Alamosa Canyon Bridge to the public. The authors would like to thank Shi-Ze Cao and Long Yang, postgraduates at Hefei University of Technology, for their kind help in the experimental test.

Reference

[1] Penna, Federico, Roberto Garello, and Maurizio A. Spirito. "Cooperative spectrum sensing based on the limiting eigenvalue ratio distribution in Wishart matrices." arXiv preprint arXiv:0902.1947 (2009).

[2] R. C. Geary, The frequency distribution of the quotient of two normal variates, Journal of Royal Statistical Society 93 (1930) 442-446.

[3] Li, J., and Chen, J.B. (2006) “The probability density evolution method for dynamic response analysis of non−linear stochastic structures.” International Journal for Numerical Methods in Engineering, 65(6), 882-903.

[4] Chen, J.B., and Li, J. (2005). “Dynamic response and reliability analysis of non-linear stochastic structures.” Probabilistic Engineering Mechanics, 20(1), 33-44.

[5] Sarrafi, A., Mao, Z., Shiao, M., 2019. Uncertainty quantification framework for wavelet transformation of noise-contaminated signals. Measurement, 137, pp.102-115.

[6] G. Marsaglia, Ratios of normal variables and ratios of sums of uniform variables. Journal of the American Statistical Association, 1965, 60: 193-204.

[7] P. J. Korhonen, S. C. Narula, The probability distribution of the ratio of the absolute values of two normal variables. Journal of Statistical Computation and Simulation, 1989, 33(3): 173-182.

[8] E. Díaz-Francés, F.J. Rubio, On the existence of a normal approximation to the distribution of the ratio of two independent normal random variables. Statistical Papers, 2013, 54(2): 309-323.

[9] S. J. Press, The t-ratio distribution. Journal of the American Statistical Association, 1969, 64(325): 242-252.

[10] Kappenman, R.F., 1971. A Note on the Multivariate t-Ratio Distribution. The Annals of Mathematical Statistics, 42(1), pp.349-351.

[11] A. P. Basu, R. H. Lochner, On the distribution of the ratio of two random variables having generalized life distributions. Technometrics, 1971, 13(2): 281-287.

[12] D.L., Hawkins, C.P. Han, Bivariate distributions of some ratios of independent noncentral chi-square random variables. Communication in Statistics-Theory and Methods, 1986, 15(1): 261-277.

[13] S. B. Provost, On the distribution of the ratio of powers of sums of gamma random variables. Pakistan Journal of Statistics, 1989, 5(2),: 157-174.

[14] T., Pham-Gia, Distributions of the ratios of independent beta variables and applications. Communications in Statistics-Theory and Methods, 2000, 29(12): 2693-2715.

[15] S. Nadarajah, A. K. Gupta, On the product and ratio of Bessel random variables. International Journal of Mathematics and Mathematical Sciences, 2005, 18: 2977-2989.

[16] Baxley, R. J., Walkenhorst, B. T., & Acosta-Marum, G. (2010, December). Complex Gaussian ratio distribution with applications for error rate calculation in fading channels with imperfect CSI. In 2010 IEEE Global Telecommunications Conference GLOBECOM 2010 (pp. 1-5).

[17] Antoni, J. (2006). "Leakage-free identification of FRF's with the discrete time Fourier transform." Journal of sound and vibration, 294(4), 981-1003.

[18] Pintelon, R., Rolain, Y., and Van Moer, W. (2003). "Probability density function for frequency response function measurements using periodic signals." IEEE Transactions on Instrumentation & Measurement, 52 (1), 61-68.

[19] W.J. Yan, W.X. Ren, Generalized proper complex Gaussian ratio distribution and its application to statistical inference for frequency response functions, Journal of Engineering Mechanics, 144(9) (2018) 04018080.

[20] Mao, Z., and Todd, M.D. (2013). "Statistical modeling of frequency response function estimation for uncertainty quantification." Mechanical Systems and Signal Processing,

38(2), 333-345.

[21] Mao, Z., and Todd, M.D. (2012). “A model for quantifying uncertainty in the estimation of noise-contaminated measurements of transmissibility.” Mechanical Systems and Signal Processing, 28, 470-481.

[22] Yan, W. J., and Ren, W. X. (2016). “Circularly-symmetric complex normal ratio distribution for scalar transmissibility function. Part I: theory.” Mechanical Systems and Signal Processing, 80, 58-77.

[23] Yan, W.J. and Ren, W.X., 2019. Two notes on “Circularly-symmetric complex normal ratio distribution for scalar transmissibility functions. Part I: Fundamentals”[Mech. Syst. Signal Process. 80 (2016) 58–77]. Mechanical Systems and Signal Processing, 133, p.106285.

[24] Yan, W. J., and Ren, W. X. (2016). “Circularly-symmetric complex normal ratio distribution for scalar transmissibility function. Part II: probabilistic model and validation.” Mechanical Systems and Signal Processing, 80, 78-98.

[25] Yan, W. J., and Ren, W. X. (2018). “Circularly-symmetric complex normal ratio distribution for scalar transmissibility function. Part III: application to statistical modal analysis.” Mechanical Systems and Signal Processing, 98, 1000-1019.

[26] Maia, N.M.M., Silva, J.M.M., Almas, E.A.M., and Sampaio, R.P.C. (2003). “Damage detection in structures: From mode shape to frequency response function methods.” Mechanical Systems and Signal Processing, 17(3), 489-498.

[27] N.M.M. Maia, R. Almeida, A.P.V. Urgueira, R.P.C. Sampaio, Damage detection and quantification using transmissibility, Mechanical Systems and Signal Processing 25 (7) (2011) 2475-2483.

[28] K. Worden, Experimental validation of a structural health monitoring methodology: part I. Novelty detection on a laboratory structure, Journal of Sound and Vibration 259 (2) (2003)

323-343.

[29] E. Papatheou, G. Manson, R.J. Barthorpe, K. Worden, The use of pseudo-faults for novelty detection in SHM, Journal of Sound and Vibration 329 (12) (2010) 2349-2366.

[30] T.J. Johnson, D.E. Adams, Transmissibility as a differential indicator of structural damage, Journal of Vibration and Acoustics 124 (4) (2002) 634-641.

[31] T.J. Johnson, R.L. Brown, D.E. Adams, M. Schiefer, Distributed structural health monitoring with a smart sensor array, Mechanical Systems and Signal Processing 18 (3) (2004) 555-572.

[32] C. Devriendt, P. Guillaume, The use of transmissibility measurements in output-only modal analysis, Mechanical Systems and Signal Processing 21 (7) (2007) 2689-2696.

[33] C. Devriendt, G.D. Sitter, P. Guillaume, An operational modal analysis approach based on parametrically identified multivariable transmissibilities, Mechanical Systems and Signal Processing 24 (5) (2010) 1250-1259.

[34] W.J. Yan, W.X. Ren, Operational modal parameter identification from power spectrum density transmissibility, Computer-Aided Civil and Infrastructure Engineering 27 (3) (2012) 202-217.

[35] W.J. Yan, W.X. Ren, An Enhanced Power Spectral Density Transmissibility (EPSDT) approach for operational modal analysis: Theoretical and experimental investigation, Engineering Structures 102 (2015) 108-119.

[36] Lin, R.M., and Zhu, J. (2006). Model updating of damped structures using FRF data. Mechanical Systems and Signal Processing, 20(8), 2200-2218.

[37] V. Meruane, Model updating using antiresonant frequencies identified from transmissibility functions, Journal of Sound and Vibration 332 (4) (2013) 807-820.

[38] G. De Sitter, C. Devriendt, P. Guillaume, E. Pruyt, Operational transfer path analysis. Mechanical Systems and Signal Processing 24(2)(2010) 416-431.

[39] Z.K. Peng, G. Meng, Z.Q Lang, W.M. Zhang, F.L. Chu, Study of the effects of cubic nonlinear damping on vibration isolations using harmonic balance method, International Journal of Non-Linear Mechanics 47 (10) (2012) 1073-1080.

[40] Yan, W.J., Zhao, M.Y., Sun, Q. and Ren, W.X., 2019. Transmissibility-based system identification for structural health Monitoring: Fundamentals, approaches, and applications. Mechanical Systems and Signal Processing, 117, pp.453-482.

[41] Yan, W.J., Yang, L., Yang, X. and Ren, W.X., 2019. Statistical modeling for fast Fourier transform coefficients of operational vibration measurements with non-Gaussianity using complex-valued t-distribution. Mechanical Systems and Signal Processing, 132, pp.293-314.

[42] Smolyak, S.A., 1963. Quadrature and interpolation formulas for tensor products of certain classes of functions. In Doklady Akademii Nauk (Vol. 148, No. 5, pp. 1042-1045). Russian Academy of Sciences.

[43] Wasilkowski, Grzegorz W., and Henryk Wo´zniakowski (1995) 'Explicit cost bounds of algorithms for multivariate tensor product problems.' Journal of Complexity 8, 337-392.

[44] Heiss, V. Winschel, Likelihood approximation by numerical integration on sparse grids. Journal of Econometrics, 2008, 144(1): 62-80.

[45] J., Bin, X. Ming, C. Yang, Sparse-grid quadrature nonlinear filtering. Automatica, 2012, 48(2): 327-341.

[46] Radhakrishnan, R., Singh, A.K., Bhaumik, S. and Tomar, N.K., 2016. Multiple sparse-grid Gauss–Hermite filtering. Applied Mathematical Modelling, 40(7-8), pp.4441-4450.

[47] He, J., Gao, S. and Gong, J., 2014. A sparse grid stochastic collocation method for structural reliability analysis. Structural Safety, 51, pp.29-34.

[48] S.C. Olhede, On probability density functions for complex varables, IEEE Trans. Inf. Theory, 2006, 52(3): 1212-1217

[49] Falsone, G., & Laudani, R. (2019). Matching the principal deformation mode method with the probability transformation method for the analysis of uncertain systems. International Journal for Numerical Methods in Engineering, 118(7), 395-410.

[50] Huang, B. and Du, X., 2006. A robust design method using variable transformation and Gauss–Hermite integration. International Journal for Numerical Methods in Engineering, 66(12), pp.1841-1858.

[51] Wang, D., Tsui, K.L. and Zhou, Q., 2016. Novel Gauss–Hermite integration based Bayesian inference on optimal wavelet parameters for bearing fault diagnosis. Mechanical Systems and Signal Processing, 72, pp.80-91.

[52] Kaarnioja, V., 2013. “Smolyak Quadrature”. Master’s thesis, University of Helsinki.

[53] G.H. Golub, J.H. Welsch, Calculation of Gauss quadrature rule, Math Comput. 1969, 23(106): 221-230

[54] Schoukens J, Pintelon R, Identification of Linear Systems: A Practical Guideline for Accurate Modelling. Pergamon Press, London, 1991.

[55] Pintelon R, Rolain Y, and Van Moer W. Probability density function for frequency response function measurements using periodic signals. IEEE Transactions on Instrumentation and Measurement. 2003; 52 (1): 61-68.

[56] Yuen KV, Katafygiotis LS, Beck JL. Spectral density estimation of stochastic vector processes. Probabilistic Engineering Mechanics 2002; 17(3): 265-272.

[57] Au SK, Operational Modal Analysis: Modeling, Bayesian Inference, Uncertainty Laws. Springer, 2017.

[58] C. R. Farrar, P. J. Cornwell, S. W. Doebling, M. B. Prime, Sturctural health monitoring studies of the Alamosa canyon and I-40 Bridges. Los Alamos National Laboratory report, LA-13635-MS, 2000.

1